

YORP-Induced Long-Term Evolution of the Spin State of Small Asteroids and Meteoroids: Rubincam's Approximation

D. Vokrouhlický and D. Čapek

Institute of Astronomy, Charles University, V Holešovičkách 2, CZ-18000 Prague 8, Czech Republic
E-mail: vokrouhl@mbox.cesnet.cz

Received September 15, 2001; revised May 10, 2002

The rotation states of small asteroids and meteoroids are determined primarily by their collisions, gravitational torques due to the Sun and planets (in the case of close encounters), and internal dissipative effects (that relax the free-precession energy toward the fundamental state of principal-axis rotation). Rubincam has recently pointed out that thermal reemission on irregular-shaped bodies also results in a torque that may secularly change both the rotation rate and the orientation of the spin axis (the so-called YORP effect). Here we pursue investigation of this effect. Keeping the zero thermal-relaxation approximation of Rubincam and the assumption of the principal-axis rotation, we study the YORP effect both for precisely determined shapes of near-Earth asteroids and also for a large statistical sample of automatically generated shapes by the Gaussian-sphere technique of Muinonen. We find that the asymptotic state of the YORP evolution is characterized by an arbitrary value of the obliquity, with higher but nearly equal likelihood of $0^\circ/180^\circ$ and 90° states. At the adopted approximation, the most typical feature of this end state of the YORP evolution is secular deceleration of the rotation rate, which means that at some instant collisions will randomize the rotation state. In a minority of cases, the final state of the obliquity evolution leads to a permanent acceleration of the body's rotation, eventually resulting in rotational fission. The YORP-induced slow evolution may also play an important role in driving the rotation state of small asteroids toward the resonances between the forced precession due to the solar torque and perturbations of the orbital node and inclination. We find that for small Themis asteroids these resonances are isolated in the relevant range of frequencies, and the YORP evolving rotation may be either temporarily captured or rapidly jump across these resonances. In contrast, the possible values of the forced precession for small Flora asteroids may be resonant with clustered, nonisolated lines of the orbital perturbation. The individual rotation histories of small Flora asteroids may be thus very complicated and basically unpredictable. We comment on possible astronomical consequences of these results.

© 2002 Elsevier Science (USA)

Key Words: minor planets; asteroids; meteors; meteoroids; rotation.

1. INTRODUCTION

Small asteroids and meteoroids acquire their rotation states at the instant of their birth as ejecta from a parent body (e.g., Love and Ahrens 1997, Glibin and Farinella 1997). At later stages, mutual collisions keep modifying the rotation state, which means that the size–distribution collisional model needs to be consistently coupled with the rotation rate–distribution model (e.g., Harris 1979, Farinella *et al.* 1992). Thus, none of the small Solar System bodies have primordial rotation states that are steady over a billion year timespan.

Though collisions represent the most extensively studied aspect of the long-term evolution of the small bodies' rotation state, other effects may be also involved. Recently, Rubincam (2000) pointed out that the thermal radiation by a surface of an irregular-shaped object results in a torque which may secularly affect both the rotation frequency and the obliquity of the spin axis. Following Rubincam's suggestion we shall speak about the YORP effect (named after Yarkovsky–O'Keefe–Radzievskii–Paddack, scientists who all contributed to this topic in the past). The corresponding time scale to change the rotation rate or obliquity is unrealistically long for asteroids larger than ≈ 20 km in size, but it becomes short enough for kilometer-sized (or smaller) bodies. The YORP effect may require a timespan comparable, or even shorter than, the collision time scale to significantly change the rotation state (\approx tens or hundreds of Myr) in this size range. For decameter-sized meteoroid precursors, the YORP time scale may even become so short that this effect would dominate over collisions (Rubincam 2000). We note in advance that this conclusion may not be certain because the strength of the YORP effect could be diminished by the finite conductivity of the meteoroid surface. This, as yet unaccounted for fact in the YORP determination will be removed in the second paper of this series. However, the YORP effect certainly continues to be an important factor for modifying the rotation state of meteoroids.

The previous "YORP facts" are important as such, since they may have interesting implications on the statistical distribution

of the rotation periods of small asteroids, occurrence of close binaries produced by rotational fission, etc. However, there is an additional and very important implication of the YORP effect related to the Yarkovsky orbital effect. Actually, both effects—the Yarkovsky effect and YORP effect—have a common physical origin, namely, the surface recoil force due to the thermal radiation of the body. The Yarkovsky effect has been studied extensively over the past few years with a number of new applications related to the transport of meteorites toward the Earth (e.g., Farinella *et al.* 1998, Hartmann *et al.* 1999, Bottke *et al.* 2000, Vokrouhlický and Farinella 2000), origin and transport of large near-Earth asteroids (e.g., Farinella and Vokrouhlický 1999, Bottke *et al.* 2001a), processes in the asteroid families (e.g., Vokrouhlický *et al.* 2001, Nesvorný *et al.* 2002, Bottke *et al.* 2001b), or the possibility of directly detecting the Yarkovsky orbital perturbations of the near-Earth asteroids (e.g., Vokrouhlický *et al.* 2000). It is well known that the Yarkovsky effect sensitively depends on the orientation of the spin axis (e.g., Rubincam 1995, 1998, Vokrouhlický 1998, 1999). This mainly applies to the diurnal variant of the Yarkovsky effect, which leads to an opposite orbital effect when the prograde rotation of the body is changed by the retrograde rotation. Frequent variations of the spin axis orientation thus diminish the resulting (accumulated) Yarkovsky orbital perturbation, and this may have important implications on the relevance of the Yarkovsky effect as described here. Note that thus far most of the developed applications of the Yarkovsky effect do not include any (or just very simplified) evolution of the spin axis orientation. We thus need to understand whether some of the past investigations of the Yarkovsky effect have to be modified if the YORP-induced evolution of the spin axis is taken into account.

In this paper we investigate in a more quantitative detail the YORP effect in Rubincam's approximation. The major restriction of this approach is that of zero thermal inertia of the surface material. Following Rubincam (2000) we shall thus assume effectively immediate thermal reemission of the absorbed energy. This assumption applies rather well for small asteroids, possibly down to hundreds of meters across, that are likely covered with a thin regolith layer. Our results for the YORP evolution of several small asteroids, for which we use a very precise shape model (mostly from the analysis of the radar ranging data), are therefore justified. We shall demonstrate that the individual YORP results, such as the asymptotic values of the obliquity and the rotation rate, depend sensitively on the shape of the asteroid so that there is "no generic YORP result." To obtain information about "average YORP results" we need a larger statistical sample of objects than the few real asteroids with accurately known shapes. To that end, we analyze YORP results for a sample of small (synthetic) asteroids generated by the Gaussian-sphere technique introduced by Muinonen (e.g., Muinonen 1996, 1998). Motivated by the analysis of the proper element dispersion in the asteroid families (e.g., Nesvorný *et al.* 2002), we shall determine the characteristic YORP results (relevant time scales, etc.) for small members of the Flora and Themis families.

As already mentioned, the YORP effect is certainly not alone in affecting the rotation state of small asteroids. Of major importance are mutual collisions and, under certain circumstances, gravitational torques due to the Sun or planets. In this paper we neglect the collisional influence on rotation, since this appears to be a complicated and, to some degree, separate problem, and we focus on the long-term dynamical effects that influence the rotation state of small asteroids. Apart from the YORP effect, we pay attention to the role of the gravitational torque due to the Sun. We show that the rate of the forced precession due to this effect may resonantly beat with planetary perturbations of the orbit. Obliquity may then undergo rapid jumps or periods of random wandering on a large scale. The possible past histories of the rotation of terrestrial planets, especially Mars, Venus, and Mercury, may give an idea about the degree of chaotic effects that are predicted here for small asteroids (e.g., Laskar and Robutel 1993). The YORP effect may be instrumental in driving the rotation state of small asteroids toward these resonant phenomena. Our analysis thus indicates that the rotation state evolution of small asteroids on a Myr time scale (or longer) may be very complicated and it that may sensitively depend on the asteroid shape (and its history, which may be sculpted by collisions).

The assumption of zero thermal inertia, used throughout this paper, is most likely violated for smaller bodies, such as decimeter- or meter-sized meteoroids, for the following two reasons: (i) these bodies likely rotate fast, and (ii) their surface is likely not insulated by regolith layer but characterized by much higher thermal conductivity (affected possibly by porosity only). We thus relegate a more detailed discussion of the YORP effect on meteoroids to the second paper in this series. In particular, we shall generalize the current YORP model by including the thermal relaxation between the absorption of the solar radiation and thermal reemission, there by relaxing the restrictive assumption of the Rubincam approximation.

In the final paper of this series, we shall investigate the YORP effect within a full-fledged formulation. This means that we shall solve numerically the complete Euler's equations for the rotation state of the body on a secularly evolving orbit in the Solar System. Gravitational torque due to the Sun, as well as the thermophysical model of the YORP effect, will be included. Initial rotation will not necessarily be constrained to the principal-axis mode.

2. THEORY

Given a skin force $d\mathbf{f}$ acting on a body at the oriented surface element $d\mathbf{S}$ with a position vector \mathbf{r} , referred to the center of mass system, we can evaluate the total torque on the whole body as

$$\mathbf{T} = \int \mathbf{r} \times d\mathbf{f}, \quad (1)$$

where the integration is assumed over the whole surface. The

recoil force $d\mathbf{f}$ due to the thermally emitted radiation is given by $d\mathbf{f} \simeq -2\varepsilon\sigma T^4 d\mathbf{S}/3$, where ε is the thermal emissivity, σ is the Stefan–Boltzmann constant, and T is the temperature. Note the minus sign due to the recoil property of the radiation effect. This formula holds for an isotropic (Lambertian) thermal emission law. Certainly this law only approximates the directional properties of thermal emission of real objects, but a more complex approach goes beyond the scope of this paper. However, an even cruder simplification, which we are going to accept, follows an estimation of the surface temperature T . In principle we need a thermophysical model for its determination. Only at the limit of zero thermal relaxation, satisfied when the surface is highly insulating, can we further approximate from energy conservation $\varepsilon\sigma T^4 \simeq (1 - A)\Phi(\mathbf{n} \cdot \mathbf{n}_0)$, if $(\mathbf{n} \cdot \mathbf{n}_0) > 0$ and the element is not shadowed by another surface element; otherwise $\varepsilon\sigma T^4 \simeq 0$. Here \mathbf{n} is the outward normal to the surface element, \mathbf{n}_0 is the direction toward the Sun, Φ is the solar flux at the distance of the body from the Sun, and A is the hemispheric albedo (Vokrouhlický and Bottke 2001). Moreover, since albedo A is typically small, and additionally a part of the radiation in the optical band is also diffusely reflected (the same directional characteristics as we assume for the thermal emission), we further approximate $(1 - A) \simeq 1$. Combining the previous results we have

$$d\mathbf{f} \simeq -\frac{2\Phi}{3c} (\mathbf{n} \cdot \mathbf{n}_0) d\mathbf{S} \quad (2)$$

(here again we set formally $(\mathbf{n} \cdot \mathbf{n}_0) = 0$ when the surface element is not illuminated or shadowed). Following the suggestion of Rubincam (2000) we additionally multiply $d\mathbf{f}$ from (2) by a “fudge factor” $2/3$ to accommodate at a very rough approximation the effect of the surface thermal inertia. Though we shall see in the next paper of this series that this approximation rather weakly expresses the inertia effect, we keep the Rubincam formulation in this paper.

The formula (2) for the infinitesimal surface force $d\mathbf{f}$ is then used in (1) to obtain the total radiative torque \mathbf{T} . For a spherical body we would have $\mathbf{r} \propto \mathbf{n}$, which together with $d\mathbf{f} \propto \mathbf{n}$ leads trivially to the conclusion that the YORP torque vanishes. However, for a body of a generically irregular shape the torque \mathbf{T} does not vanish. After we specify the way that the body’s shape is modeled, the integral in (1) is computed numerically as a sum over infinitesimal surface facets.

Assuming then the principal-axis rotation of the body, we obtain (e.g., Rubincam 2000)

$$\frac{d\omega}{dt} = \frac{T_s}{C}, \quad \frac{d\epsilon}{dt} = \frac{T_\epsilon}{C\omega} \quad (3)$$

for the rate of change of the rotation angular velocity ω and the obliquity ϵ (hence $\cos \epsilon = \mathbf{N} \cdot \mathbf{s}$, with \mathbf{N} normal to the orbital plane and \mathbf{s} the spin axis). Here C is the principal moment of

inertia around the spin axis and we define

$$T_s = \mathbf{T} \cdot \mathbf{s}, \quad T_\epsilon = \mathbf{T} \cdot \mathbf{e}_\perp, \quad (4)$$

and $\mathbf{e}_\perp = (\mathbf{s} \cos \epsilon - \mathbf{N})/\sin \epsilon$. Note a difference between our variables and those used by Rubincam (2000). Namely, we systematically refer the projections T_s and T_ϵ of the YORP torque \mathbf{T} to the *spin vector* (a unit vector of the rotational angular momentum) and not to the body axis \mathbf{e}_z (hence we prefer the notation T_s instead of T_z used by Rubincam). When the sense of rotation is changed, or in other words the spin axis is inverted with respect to the body ($\mathbf{s} \rightarrow -\mathbf{s}$), the YORP torque \mathbf{T} and the projection T_ϵ do not change their sign but the projection T_s does change sign. With Eqs. (3) this means that when the spin axis is inverted with respect to the body the rotation is accelerated in one case and decelerated in the other; the effect on obliquity is also reversed, since the axis inversion means the obliquity transformation $\epsilon \rightarrow 180 - \epsilon$. Another symmetry, involving averaging over a circular orbit, will be discussed in the following.

Let us emphasize our *assumption* that the internal processes resulting in dissipation of the free-wobble energy are strong enough to maintain the shortest axis rotation state. In Section 3.3 we shall summarize the current knowledge of the strength of these dissipative effects and we shall give the corresponding time scale to align the generic rotation state toward the lowest energy state. Note, however, that the YORP effect tends to destroy the principal-axis rotation, since the projection of YORP torque on all axes in the body frame are of comparable magnitude. This is still true for the averaged quantities discussed in the following. Only if the YORP evolution time scale were (much) longer than the estimated time scale for the wobble dissipation would principal-axis rotation be justified. We shall see that this is true for multikilometer-sized asteroids, but it becomes questionable for kilometer-sized objects. A thorough analysis of the YORP effect in the non-principal-axis rotation state, with the YORP contribution used to trigger this state, is beyond the scope of this introductory paper. The third paper in this series will be devoted to this problem.

Since we are interested in the long-term evolution of the rotation state, it is appropriate to average T_s and T_ϵ in the right-hand sides of (3) over both rotation and revolution cycles. This procedure may require care in the case of a very slow rotation, but in the majority of cases of interest the rotation period is several orders of magnitude smaller than the revolution period. The double averaging can therefore be performed in rotation and revolution phase angles independently. Unlike in the case of the torque due to the direct (absorbed) solar radiation pressure, the YORP torque does not average to zero. For circular orbits, assumed throughout this paper, the resulting averaged torques \bar{T}_s and \bar{T}_ϵ depend on the obliquity ϵ . In the case of an eccentric orbit the phase angle of the spin axis projection onto the orbital plane would appear as a second parameter of the $(\bar{T}_s, \bar{T}_\epsilon)$ torques.

In assuming a circular orbit, we should notice another “symmetry” related to the spin axis inversion (not identical, however,

to that just discussed). For a *conserved* sense of rotation, or in other words a conserved position of the spin axis in the body-fixed frame, we may be willing to investigate how the *averaged* torques \bar{T}_s and \bar{T}_ϵ change at the inversion of the spin axis in space. For a given instant of the revolution around the Sun, this operation results in a different value of the YORP torque, since a different part of the body's surface is illuminated. However, there is a symmetric configuration, as far as the surface illumination is concerned, after half revolution on the circular orbit. The YORP torque projected onto the body-fixed axes is the same, and thus so is the T_s quantity, but the T_ϵ variable changes its sign. As a result, the obliquity transformation $\epsilon \rightarrow 180 - \epsilon$, with the conserved orientation of the spin axis in the body-fixed frame, results in the following (anti)symmetry of the averaged YORP torques: $\bar{T}_s(180 - \epsilon) = \bar{T}_s(\epsilon)$ and $\bar{T}_\epsilon(180 - \epsilon) = -\bar{T}_\epsilon(\epsilon)$. Note also the fine difference between this symmetry and the one accompanied by the spin axis inversion in the body-fixed frame. In the latter case both $\bar{T}_s(\epsilon)$ and $\bar{T}_\epsilon(\epsilon)$ change their sign.

Throughout the text we assume that the averaging approach is applicable. In the real astronomical situations we have in mind, this constrains the rotation period to be smaller than a few months (a constraint that is essentially always satisfied). We shall see in the following that the YORP evolution may result in an asymptotic phase characterized by a permanent despinning of the rotation. We should thus keep in mind that the adopted approximation, based on the averaging technique, does not allow us to extrapolate this asymptotic phase too long. However, such long periods are probably not relevant because of collisional evolution, which is also neglected in this paper.

Adopting the preceding physical approximations we realize that the appropriate modeling of the irregular shape of the body is the most important issue. In the next two sections we briefly explain our approach in this respect. We investigate about a dozen cases of small asteroids for which the shapes are accurately known. Unfortunately, this represents too small a sample for characterizing statistically the YORP effect on the long-term spin dynamics of asteroids. Therefore, in Section 2.2 we recall a powerful technique for generating irregular-shaped (synthetic) objects with mean characteristics fitting small asteroids. This will allow us to produce a larger sample of objects for which we may determine the “mean YORP effect” on their rotation state.

2.1. Polyhedral Model of the Asteroid Shape

Though the ellipsoidal shape model for small asteroids is by far the most common and was thus used for computing their lightcurves in majority of cases, real asteroids typically indicate a much higher degree of irregularity. In addition, the fact that the YORP effect depends sensitively on the asteroid shape, as already noted by Rubincam (2000), prompts us to use a more accurate shape model.

There are basically two approaches that are often used for describing of an arbitrarily shaped body: (i) spherical harmonics development of the distance $r(\theta, \phi)$ toward the surface along

the direction characterized by the spherical angles θ and ϕ , and (ii) polyhedral model consisting of a list of surface vertexes and their identification as infinitesimal surface elements (facets). Both methods have been used for shape modeling of planetary satellites and small asteroids. The polyhedral model is clearly a more general tool (e.g., Simonelli *et al.* 1993). First, fine surface structures (such as crater morphology or linear faults) are difficult to accommodate into a “reasonable-degree” spherical model; yet they may have influence on the exact value of the YORP torque. Second, the most irregular shapes cannot even be described by a single series within the spherical harmonic approach, since there might be several surface facets seen along a given direction from the center of mass. This situation occurs, for instance, in the case of the asteroids Kleopatra and Geographos. These reasons led us to use the polyhedral model description of the asteroid shape in this paper. A practical bonus is the fact that the best-determined shapes of the near-Earth asteroids (except Eros), acquired by radar ranging, are directly exported in this format. We thus use data of six detailed asteroidal shapes available from <http://echo.jpl.nasa.gov/links.html> (their polyhedral approximation contains typically 4092 surface elements; the finest model of Toutatis has 12,796 surface elements). The polyhedral model of asteroid 6053 (1993BW3) is taken from Āurech (2002). Additionally, we use data on asteroids and martian satellites acquired through satellite observations and available as spherical harmonics models [e.g., 24-degree Eros data are available from <http://near.jhuapl.edu/> (see also Yeomans *et al.* 2000) and a six-degree Deimos model is taken from Rubincam *et al.* 1995]. In each of these cases we have transformed the original data to a polyhedral model with typically 4000 surface elements. We started with nodes given by even coverage of a sphere in latitude and longitude but then iterated nodal positions so that the surface elements have approximately the same area.

Given the goal of our study, we need to compute a number of physical parameters of the studied objects: total mass (volume), surface area, inertia tensor, etc. For that purpose we basically follow the paper by Dobrovolskis (1996), generalizing it for a few complicated cases with several surface facets in a given (single) direction in the center of mass system.

A particular problem we faced when computing the YORP torque is that of illumination of a given surface facet. Given a frequent concave shape of small objects, there exists a possibility that some surface elements may produce a shadow which prevents illumination of other surface elements. Interestingly, a similar problem is encountered in satellite geodesy, in particular for accurate determination of the atmospheric and radiation drag on irregular-shaped artificial satellites. The most precise approach, notably the individual ray-tracing technique (e.g., Klinkrad *et al.* 1990), is typically a rather time-consuming procedure. We have thus chosen a compromise between the computational accuracy and computer-time demands. For all surface elements we precomputed a list of other, potentially shadowing facets. The minimum local zenith angle is also precomputed and

stored in computer memory. A special test is then performed when a potentially shadowing situation is detected in the course of computing the YORP effect. Notably, we investigate whether centers of the potentially shadowing facets are projected onto the given surface element (as seen from the solar direction).

At a still higher degree of precision one should take into account self-irradiation of the irregular shape (i.e., thermal radiation from one surface facet can illuminate another facet and thus produce a corresponding radiation pressure). The ray-tracing technique can tackle complexities of this kind, but we neglect this effect in this study.

The precision with which we can compute the averaged values of the YORP torques \bar{T}_s and \bar{T}_c is limited mainly due to finite area of the surface facets (modeled as planar). However, we have verified that by taking more than 1000 facets, as we always do, the YORP torques can be computed with at least 1% precision in all our cases. The fact that the computed quantities are averaged over the rotation and revolution cycles helps to diminish the error of numerical evaluation of the resulting torques.

2.2. Gaussian Random Spheres

Muinoen (1996, 1998), following previous studies of the Finnish school dealing with light scattering on small, irregular dust particles, pointed out that the Gaussian-sphere model is a robust scheme for describing shapes of small Solar System objects (asteroids and comets). Within this model, radii of a large sample of the objects satisfy log-normal statistics with a variance σ and a characteristic dimensional factor a (if properly scaled). In the center of mass system the radius $r(\theta, \phi)$ in a direction given by spherical angles θ and ϕ may be expressed as

$$r(\theta, \phi) = \frac{a}{\sqrt{1 + \sigma^2}} \exp[s(\theta, \phi)], \quad (5)$$

where the $s(\theta, \phi)$ function obeys spherical harmonic development,

$$s(\theta, \phi) = \sum_{\ell=0}^{\infty} \sum_{m=0}^{\ell} P_{\ell}^m(\cos \theta) (a_{\ell m} \cos m\phi + b_{\ell m} \sin m\phi). \quad (6)$$

The coefficients $(a_{\ell m}, b_{\ell m})$ of these series are independent Gaussian random variables with zero mean and variance reading

$$\beta_{\ell m}^2 = (2 - \delta_{\ell 0}) \frac{(\ell - m)!}{(\ell + m)!} c_{\ell} \beta^2, \quad (7)$$

with $\beta^2 = \ln(1 + \sigma^2)$ and $\delta_{\ell 0}$ the Kronecker symbol. The model then depends on the variance σ of the distribution of surface heights and on a set of parameters c_{ℓ} from (7). These latter parameters describe how the height anomalies fluctuate over the sphere, or more precisely they describe autocorrelation of the log radii for a given angular distance of two surface elements. A convenient single parametric choice for this autocorrelation function was suggested by Muinoen (1996); the sec-

ond Gaussian-sphere model parameter is then Γ , the correlation angle of the surface fluctuations. This model was later generalized by Muinoen (1998), who constructed the autocorrelation function of surface heights at given angular distance by a linear combination of two different functions of Γ (the weighting factor represents then an additional parameter of the model).

The most relevant, in our context, is then the work by Muinoen and Lagerros (1998). These authors analyzed accurately known shapes of 14 asteroids to verify whether they satisfy the Gaussian-shape hypothesis. They obtained the best estimates of the parameters (σ, Γ) for their sample of asteroids, and also for a subset of 7 small asteroids (with sizes smaller than 10 km). In what follows we generate a large sample of ‘‘synthetic’’ shapes of small asteroids, represented by the Gaussian spheres with the previously mentioned parameters determined by Muinoen and Lagerros (1998) for small asteroids. Notably, we have $\sigma = 0.274$ and $\Gamma = 30.9^\circ$; in fact we consider directly the values of c_{ℓ} as determined by Muinoen and Lagerros (1998) and accept a cut-off at $\ell = 10$ (see Table 5 of this reference). The scale parameter a , in Eq. (5), is obviously arbitrary and we typically fix its value at 1 km. As already indicated, we then convert each of the generated objects in the finite-element triangulation of the surface (polyhedral model); for the sake of statistical tests that follow we use 1004 surface elements. Figure 1 shows four typical synthetic asteroids in our sample.

Figures 2 and 3 show distribution of the dynamical ellipticity $(C - (A + B)/2)/C$ and the triaxiality factor A/B for a sample of 1000 Gaussian random spheres generated by this procedure. Symbols indicate the values of the same parameter for the few real asteroids (and Deimos) with accurately known shape. Figure 2 confirms that the small Solar System objects are significantly different from spheres with a typical dynamical

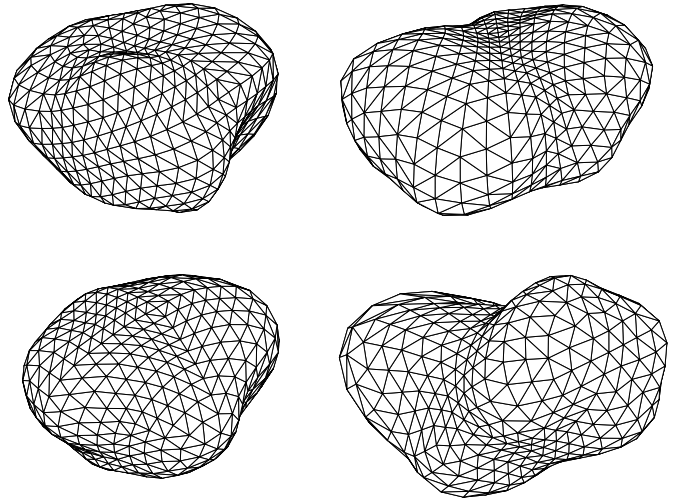


FIG. 1. Typical shapes of four synthetic asteroids generated by the Gaussian-sphere method; statistical parameters of the model correspond to those determined for small asteroids by Muinoen and Lagerros (1998). Each of the objects is represented by a polyhedral model with 1004 surface elements.

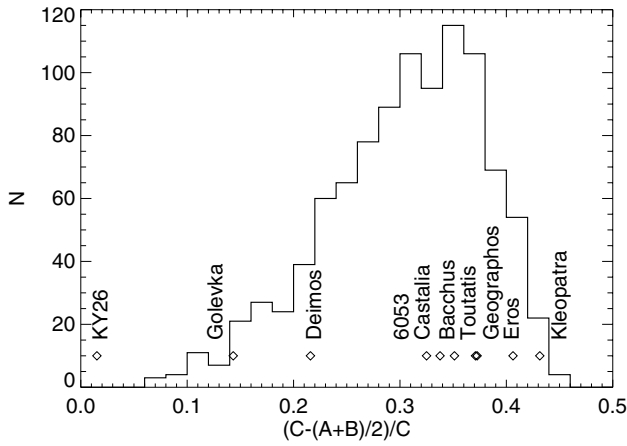


FIG. 2. Distribution of the dynamical ellipticity $(C - (A + B)/2)/C$ for a set of 1000 generated artificial objects by the technique described in the text. The peak value is at about 0.3; symbols denote values of this parameter for the nine asteroids and Deimos, for which we have precise shape models from the inversion of the radar data or satellite observations.

ellipticity value of ≈ 0.3 . The distribution of both variables for the synthetic Gaussian spheres represents relatively well the density determined from real asteroid data. This confirms that our synthetic asteroids describe the asteroid population realistically. A curious exception is the ≈ 30 -m-sized asteroid 1998KY26 (Ostro *et al.* 1999b).

3. RESULTS AND DISCUSSION

Hereafter we shall demonstrate the possible diversity of the YORP results through the parameter dependence of the averaged torques \bar{T}_s and \bar{T}_ϵ [see Eqs. (4)]. In particular, we find that the YORP effect on these few asteroids, which basically differ just by their shape, may span all possible combinations of results.

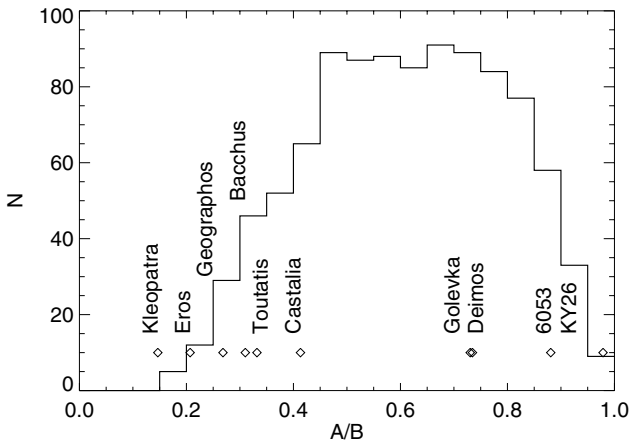


FIG. 3. Distribution of the triaxiality parameter A/B for a set of 1000 generated artificial objects by the technique described in the text. The peak value is at about 0.7; symbols denote values of this parameter for the nine asteroids and Deimos, for which we have determined precise shape models from the inversion of the radar data or satellite observations.

After classifying these individual results, essentially according to the dependence of \bar{T}_ϵ on the obliquity (with circular orbits assumed), we perform a statistical study to understand which of the different cases is the most typical. To that purpose we use a sample of 500 Gaussian random spheres generated as described in Section 2.2.

Though we use shapes of real (mostly near-Earth) asteroids we relegate the results to a single value of distance from the Sun, notably 2.5 AU. It is easy to understand from Eq. (2) that the results for the averaged torques scale as $\propto 1/d^2$, with d being the mean distance from the Sun. Similarly, though in all cases of real asteroids we keep their true dimensions, it is easy to see that \bar{T}_s and \bar{T}_ϵ scale as $\propto 1/L^2$, where L is the linear scale of the object. In the case of a statistical sample of Gaussian spheres (Section 3.1.5), we set $a = 1$ km for the scale parameter in Eq. (5). If qualitative results are reported, we always assume homogeneous bodies with a density of $\rho = 2.5$ g/cm³. If another density is more appropriate, such as for the C-type asteroids, the magnitude of the YORP torques scales as $\propto 1/\rho$.

3.1. Examples of the YORP Results

3.1.1. Type I: Eros, 1998KY26, 6053, and Toutatis

Figure 4 shows the averaged YORP torques \bar{T}_s/C and \bar{T}_ϵ/C from the right-hand sides of Eqs. (3) for an Eros-shaped object at 2.5 AU. Obviously, we adopt the real orientation of the spin vector in the Eros' body-fixed frame as it corresponds to the real asteroid; only the obliquity (today's value for Eros is $\approx 82^\circ$) is allowed to span the entire $(0, 180)$ degree interval. As already discussed, the averaged YORP torques then satisfy the following properties of (anti)symmetry: $\bar{T}_s(\epsilon) = \bar{T}_s(180 - \epsilon)$ and $\bar{T}_\epsilon(\epsilon) = -\bar{T}_\epsilon(180 - \epsilon)$. The result from Fig. 4 corresponds to that of Rubincam (2000) qualitatively, but as far as the quantitative value is concerned Rubincam indicates YORP torques ≈ 3 times larger. We have checked our result several times and believe that it is correct. Nonetheless, this minor difference

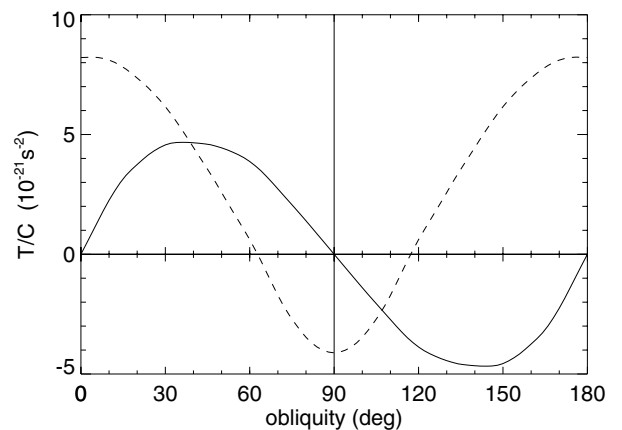


FIG. 4. Obliquity dependence of the averaged YORP torques \bar{T}_s (dashed line) and \bar{T}_ϵ (solid line) for an Eros-shaped object at a circular orbit with radius of 2.5 AU. The torques are divided by the principal moment of inertia C .

cannot change any of the conclusions from either our or Rubincam’s work. Notice, in particular, that the positive value of \bar{T}_ϵ in the $(0^\circ, 90^\circ)$ obliquity range means that the YORP evolution always asymptotically reaches $\epsilon_f = 90^\circ$ obliquity. Since \bar{T}_s is negative at this value of obliquity, the final state of the YORP evolution corresponds to a permanent deceleration of the rotation. Note, however, that \bar{T}_s is positive up to obliquity of 62° , which means that in the course of the YORP evolution the body may undergo a phase of spinning up of its rotation. This evolution characterizes type I cases in our classification. A similar result was found for asteroids 1998KY26 and 6053 (1993BW3), and Rubincam (2000) reports the same result for Gaspra and Ida.

The strength of the YORP effect may be illustrated in the case of the small asteroid 1998KY26. Rubincam (2000) argued that a characteristic time scale for doubling the rotation period is given by $\approx C\omega/\bar{T}_s$. Applying this estimation to 1998KY26 with a mean value of $\bar{T}_s \approx 10^{-15} \text{ s}^{-2}$, we obtain a doubling of its rotation period in only $\approx 10^4$ years. This is a surprisingly short time. We anticipate that a more complete YORP model, which includes the effects of the thermal inertia of the surface (which is neglected here but is likely for such a small object), may prolong this time scale by a factor ≈ 10 – 100 . Still, a 0.1–1 Myr timespan to significantly alter the rotation state of 1998KY26 (or similar objects) is smaller than the dynamical lifetime of its orbit. It is also interesting to note that the rotation period of 1998KY26 has been measured with $\simeq 4 \times 10^{-5}$ fractional uncertainty during the 1998 observational campaign. Considering our result, its fractional change due to the YORP effect in 26 years, at the next close approach to the Earth in May 2024, is expected to be $\simeq 5 \times 10^{-3}$. We thus predict that the YORP effect is likely to be observable for this object. The previous conclusion also confirms that the YORP effect should still be important for obliquity evolution of the meteorite precursors. Implications of this fact in a combined model with their Yarkovsky delivery toward the Earth (e.g., Bottke *et al.* 2000, Vokrouhlický and Farinella 2000) needs to be studied in the future.

Finally, we mention that the YORP effect on a Toutatis-shaped object was found of this type I (Fig. 5). We should, however, recall that here we assumed the principal-axis rotation of a Toutatis-shape object. Rather than indicating the YORP effect on the real Toutatis we are thus reporting a result for a fictitious asteroid of the same shape (Toutatis is presently in a tumbling rotation state; Ostro *et al.* 1999a). An interesting feature of the YORP solution of the principal-axis rotator of the Toutatis-shaped body is a permanent deceleration of the rotation period (\bar{T}_s is always negative).

3.1.2. Type II: Deimos and Kleopatra

Deimos presents an inverted case of the Eros results (see Fig. 6); namely, \bar{T}_ϵ is negative in the $(0^\circ, 90^\circ)$ obliquity range. As a result, the asymptotic obliquity value of the YORP evolution is $\epsilon_f = 0^\circ$ (or 180° , depending on the initial value of ϵ). The asymptotic despinning of the rotation ($\bar{T}_s(0) < 0$ and $\bar{T}_s(180) < 0$) is a common feature with the previously discussed type I cases.

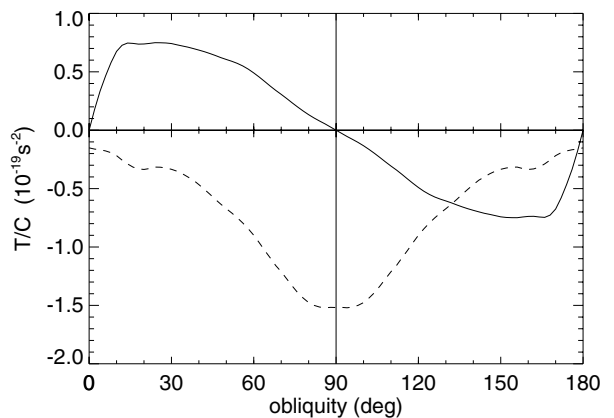


FIG. 5. The same as in Fig. 4, except for a Toutatis-shaped object rotating along its shortest principal axis.

Rubincam (2000) noticed this “anomalous” behavior of YORP on Deimos, but he artificially inverted the rotation axis with respect to the body (or the sense of its rotation). He rightly noted that the inversion causes Deimos to despin rather than to spin up its rotation for the given value of the obliquity, but he missed the point that the asymptotic YORP state is despinning in both cases.

The YORP effect on Kleopatra is qualitatively the same as for Deimos, but its larger size makes the YORP effect on this particular body negligible. The YORP time scale to double Kleopatra’s rotation period is of the order of 1000 Gyr, an entirely irrelevant number from the astronomical point of view. However, a kilometer-sized object of Kleopatra’s shape would double its rotation period in ≈ 100 Myr only (thanks to the quadratic scaling of the YORP torques in the objects size).

3.1.3. Type III: Castalia and Geographos

The third type of our classification is represented by Castalia (see Fig. 7). The value of \bar{T}_ϵ is positive up to some critical value ϵ_* of the obliquity, while for large values it becomes negative

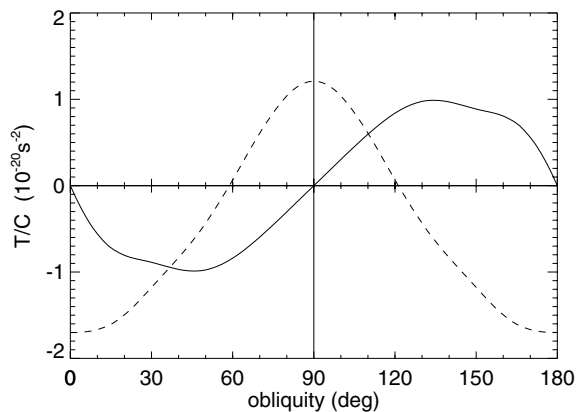


FIG. 6. The same as in Fig. 4, except for a Deimos-shaped object.

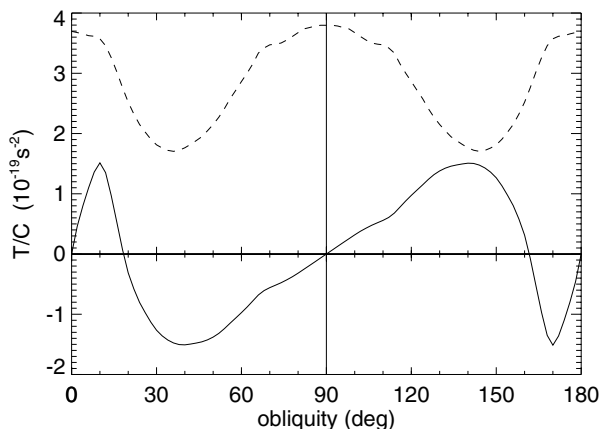


FIG. 7. The same as in Fig. 4, except for a Castalia-shaped object.

($\epsilon_* \simeq 30^\circ$ for Bacchus). This means that ϵ_* (or $180 - \epsilon_*$) is the asymptotic value of obliquity that is reached by the YORP evolution at large time. Castalia's peculiarity is because the \bar{T}_s torque is always positive. This latter fact means that the YORP effect permanently accelerates the body's rotation. This finding is interesting, since there is apparently a single outcome of this evolution, namely, rotational fission. Obviously, in particular cases we should investigate the corresponding time scale needed to reach the fission state. For instance, in Castalia's case we have estimated that its ≈ 4 -h rotation will reach ≈ 2 h, an approximate disruption limit, in about 10 Myr. Though this estimation of the time scale for doubling Castalia's rotation frequency is not much longer than the estimated dynamical lifetime of its orbit (tens to a hundred million years), and thus it is astronomically relevant, it needs to be validated within a more general model (including eccentricity of Castalia's orbit, possible changes in its shape when approaching the critical rotation limit, deviation from the principal-axis rotation state, etc.). Castalia's rotational fission may also be facilitated by the fact that the cohesion at the junction of the two lobes of this asteroid, believed to be small asteroids that collided in a "subcatastrophic way" (e.g., Ostro *et al.* 1989), may be little lower. In any case, Castalia's result indicates that the YORP-induced bursting of small Solar System objects (see Rubincam 2000) may indeed occur in some special cases. Recall that this was the original motivation for studying the radiation torques (e.g., Radzievskii 1954, Paddack 1969).

The YORP effect on Geographos resembles closely that of Castalia (see Fig. 8). The \bar{T}_s is nearly always positive. Geographos' rotation is thus virtually always accelerated. One easily estimates that the Geographos rotation frequency doubles in about 50 Myr. Again, though interesting, this number needs to be validated by a more precise model as already outlined. Geographos is thought to have undergone a "recent" close approach to the Earth that modified both its shape and its rotation state (e.g., Bottke *et al.* 1999). Such events are rare enough that the YORP effect may secularly change its rotation state before the next deep encounter, but the ≈ 10 - to 100-Myr dynamical lifetime of the Geographos orbit may prevent a significant effect.

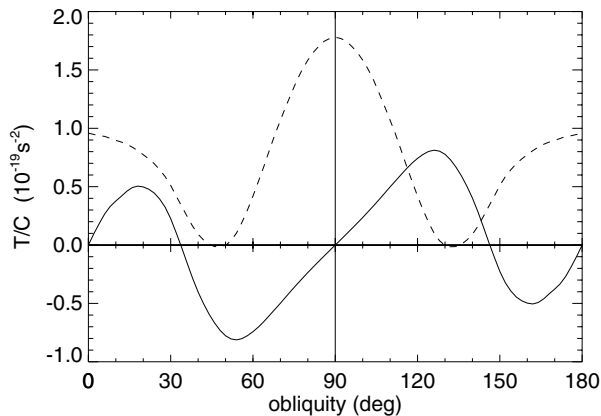


FIG. 8. The same as in Fig. 4, except for a Geographos-shaped object.

Anyway, we found it interesting that the sub-kilometer-sized near-Earth asteroids have YORP time scales (to double the rotation frequency) comparable to their dynamical lifetimes.

3.1.4. Type IV: Golevka and Bacchus

The final type of our classification is again characterized by a single node of \bar{T}_ϵ in the $(0^\circ, 90^\circ)$ obliquity range. An example is given by Golevka, whose averaged YORP torques are shown in Fig. 9. The YORP effect drives the obliquity either to 0° (or 180°) or to 90° depending on the initial state. Assuming a random initial state, there is $(\cos \epsilon_*)$ probability that 0° will be a final state obliquity; as before, ϵ_* is the node of $\bar{T}_\epsilon(\epsilon) = 0$. Interestingly, the rotation rate behaves in a different way for the two possible asymptotic states; namely, it decelerates at 0° (and 180°) and accelerates at 90° . An inverse asymptotic behavior is observed in the Bacchus case (Fig. 10).

In the case of the real asteroidal shapes studied here we did not encounter a situation going beyond our classification, notably with more than one node of $\bar{T}_\epsilon(\epsilon)$ in the $(0^\circ, 90^\circ)$ obliquity range. In principle, this may not be excluded, but it appears less common. Occasionally, two nodes of \bar{T}_ϵ were observed

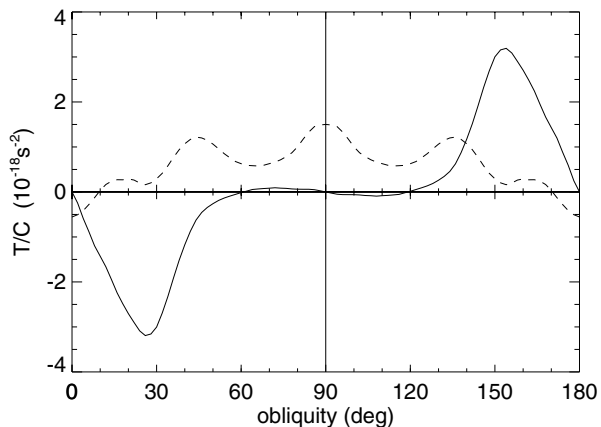


FIG. 9. The same as in Fig. 4, except for a Golevka-shaped object.

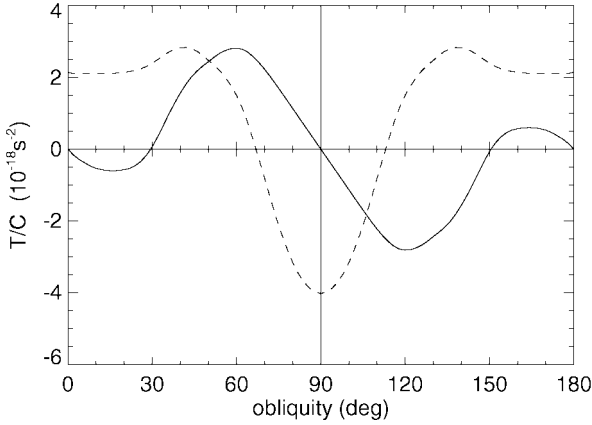


FIG. 10. The same as in Fig. 4, except for a Bacchus-shaped object.

among the randomly generated shapes discussed in the next section.

3.1.5. Statistical Results for a Sample of Gaussian Spheres

The quantitative values, though interesting in particular cases, are not the most important conclusion from the previous sections. Rather, we would like to point out the diversity of the YORP results despite the very restricted (and randomly chosen) sample of objects taken into account. This means that there is no “generic” YORP result. We have seen that the obliquity may be driven to any value (with probably a slight preference to 0° , 90° , and 180°) and the asymptotic states may be characterized by either deceleration or acceleration of the rotation rate (with more likely the case of despinning). In several applications, mostly related to the Yarkovsky orbital perturbations on a large sample of “individually undefined” objects, we might be interested in a statistical description of the YORP results. This is the case of understanding the role of the Yarkovsky effect in meteorite or near-Earth asteroid delivery (e.g., Farinella and Vokrouhlický 1999, Bottke *et al.* 2000, 2001a, Vokrouhlický and Farinella 2000) or Yarkovsky-driven diffusion processes in the asteroid families (Nesvorný *et al.* 2002, Bottke *et al.* 2001b). For this purpose we computed the YORP torques on a sample of 500 Gaussian random spheres generated by the Muinonen technique briefly recalled in Section 2.2. All bodies have an equivalent radius of 1 km, have a mean density of 2.5 g/cm^3 , and are assumed to move on a circular orbit at 2.5 AU from the Sun.

Figures 11 and 12 show the \bar{T}_ϵ and \bar{T}_s torques, each for 30 and 10 typical objects (more data would make the figures too busy). To better explore the results we distinguish the different cases according to our previous classification; namely, Fig. 11 shows 30 type I and II results and Fig. 12 shows 10 type III and IV results. We found that the abundance of the type I and II cases is approximately the same, 39.2% and 40.4%, while type III and IV cases occur statistically less frequently (only 10.2 and 6.2% of all cases). As previously, mentioned, we have also occasionally identified peculiar cases with two nodes of \bar{T}_ϵ

in the $(0^\circ, 90^\circ)$ obliquity range that cannot be fit into any of the four classes—there were 20 such cases in the sample of 500 generated objects. In principle, the number of these nodes is not limited and the likelihood of the complicated cases decreases quickly with number of nodes. Since the classification is not a substantial result of our paper (rather it is a mean to more easily distinguish different possible results), we do not extend the classification given here for these more complicated cases.

Separating the results according to the classes introduced here fixes the behavior of the \bar{T}_ϵ torque, but it does not constrain the \bar{T}_s torque. Figures 11 and 12 indicate that the *asymptotic deceleration* of the rotation frequency is statistically much more likely than its acceleration (here “asymptotic” means at the obliquity value toward which YORP drives the spin axis at long term, i.e., 90° for the type I and 0° or 180° for the type II solutions). This result may look peculiar, but we want to warn the reader not to draw hasty conclusions. We have carefully checked that there is an equal likelihood of positive value of T_s moment at a given point on the orbit among the sample of the randomly

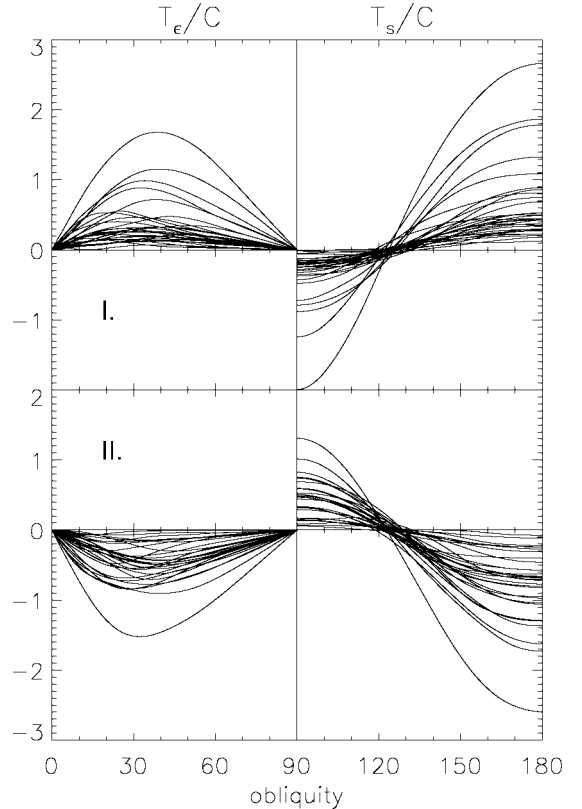


FIG. 11. Behavior of the $\bar{T}_\epsilon(\epsilon)/C$ (left, $\epsilon \leq 90^\circ$) and $\bar{T}_s(\epsilon)/C$ (right, $\epsilon \geq 90^\circ$) for a randomly chosen 30 cases from the sample of Gaussian spheres. The values in the complementary parts of the obliquity interval follow from the obvious symmetries $\bar{T}_\epsilon(180 - \epsilon) = -\bar{T}_\epsilon(\epsilon)$ and $\bar{T}_s(180 - \epsilon) = \bar{T}_s(\epsilon)$. The upper part of the figure corresponds to the type I solutions, while the lower part of the figure corresponds to the type II solutions. The ordinate units are 10^{-18} s^{-2} . Note that in both cases there is an asymmetry in the asymptotic deceleration/acceleration of the rotation frequency toward deceleration.

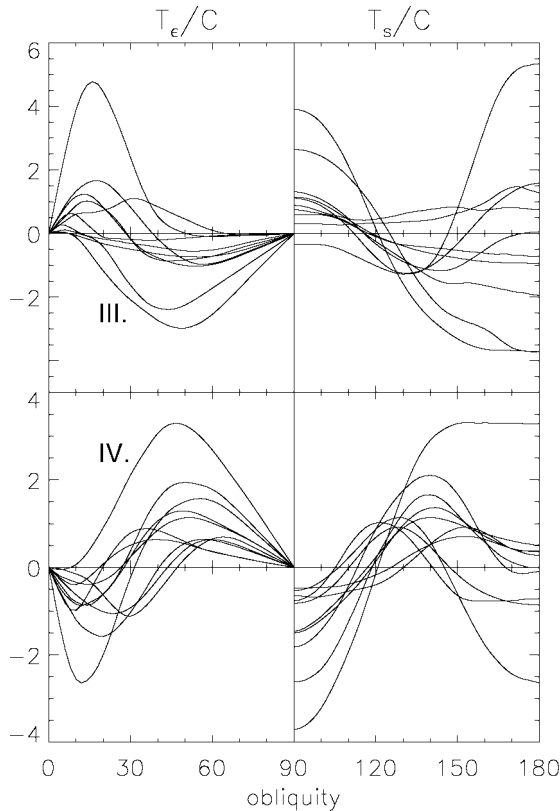


FIG. 12. The same as in the Fig. 11, except for for 10 randomly chosen type III and IV results (more examples would make the figure too busy). The ordinate units are 10^{-19} s^{-2} .

generated asteroids (even when we average over the rotation cycle). This finding fits the intuitive idea that might be gained, for instance, from Fig. 1 in Rubincam (2000): YORP may equally well accelerate or decelerate the rotation (imagine two senses of rotation of the windmill-shaped asteroid). But here we refer on the asymmetry of the YORP effect at the asymptotic value of its long-term evolution (and, moreover, averaged over both the rotation and revolution cycles). This is by no means an intuitive quantity, and we in fact did not find such an easy argument in favor of our result (except a careful check of our code). A part of this problem may also be that our representation is actually not entirely complete; as mentioned in Section 2 the YORP naturally drives the rotation from the principal-axis state. The statistics of the asymptotic rotation at the final state therefore need to be substantiated within a more complete model in the future.

Note that within one type there is a significant scatter of the magnitude of the YORP effect between the minimum and maximum strengths. Obviously, more “regular” objects are subject to a smaller effect while YORP is larger for more irregular-shaped objects. In Section 2 we recalled a trivial result, that the YORP effect is nil for spherical bodies. It can however, be easily shown that the averaged torques $\bar{T}_s(\epsilon)$ and $\bar{T}_\epsilon(\epsilon)$ vanish for triaxial ellipsoids (see Rubincam 2000). Figure 13 shows the distribution of the maximum values of $\bar{T}_\epsilon(\epsilon)$ for obliquities within the $(0^\circ, 90^\circ)$

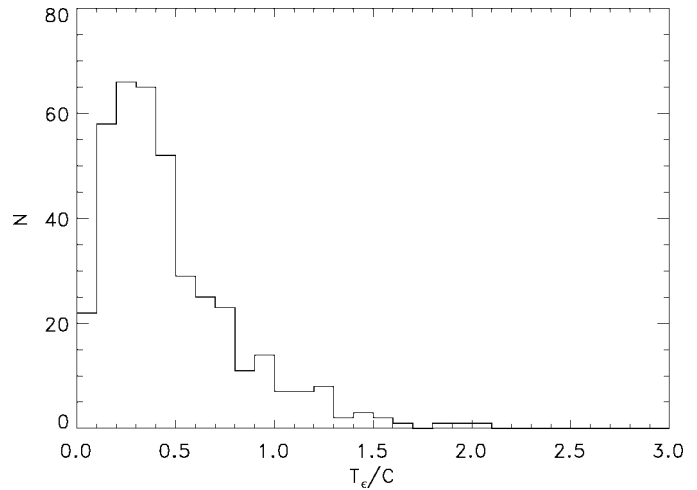


FIG. 13. Distribution of maximum values of \bar{T}_ϵ/C for type I and II cases among the sample of 500 Gaussian random spheres. Abscissa units are 10^{-18} s^{-2} .

range for the population of 196 identified type I cases from the entire sample of 500 Gaussian spheres. Although the spherical bodies are statistically absent in our sample (Fig. 2), a relative “excess” of small values in Fig. 13 is caused by objects with shapes that are rather well approximated by an ellipsoid.

Figure 14, showing the distribution $p(\epsilon)$ of the asymptotic obliquity values from the whole sample of objects, confirms that the values 0° (and 180°) and 90° are dominant. The intermediate values, corresponding to the type III class, represent a minority of cases (in total only 6.3%). When constructing $p(\epsilon)$ we assume a random initial orientation of the spin axis. This means, for instance, that in the case of the type IV solution we assign $(\cos \epsilon_*)$ probability of the 90° asymptotic solution of the obliquity and $(\sin^2(\epsilon_*/2))$ probabilities to 0° and 180° asymptotic values of the obliquity. The results indicate that the likelihood of the 90° (“in-plane”) asymptotic obliquity is about the same as the sum of the

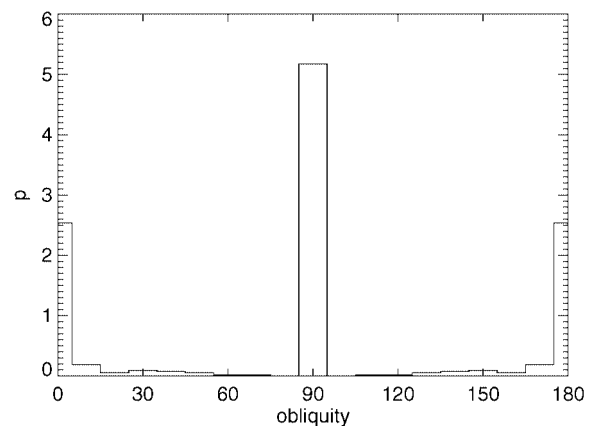


FIG. 14. Distribution $p(\epsilon)$ of the asymptotic obliquities of the YORP evolution for the sample of 500 Gaussian random spheres. The maximum of the distribution is normalized such that the integral $\int_0^\pi dep(\epsilon) \sin \epsilon$ is unity.

0° and 180° (“perpendicular”) asymptotic states. The majority of these cases are produced by the type I and type II cases.

As mentioned in Section 1, the Yarkovsky effect, together with a slow chaotic diffusion, may significantly influence dispersion of (small) members of the asteroid families and thus help to reconcile inconsistency between the velocity fields inferred from the families and those from the hydrocode simulations (see Nesvorný *et al.* 2002, Bottke *et al.* 2001b). Together with the problem of leaking of small asteroids from the main belt (e.g., Farinella and Vokrouhlický 1999, Bottke *et al.* 2001a), the histories of asteroid families strongly motivate understanding of the spin axis evolution of the kilometer-sized asteroids.

Given this motivation, and using the YORP data on the sample of 500 Gaussian random spheres, we may investigate several interesting problems. For instance, we sought the characteristic YORP time scale to reach the slow-rotation state for the small members of the asteroid families in the main belt. Starting with a generic orientation of the spin axis, assumed isotropic in space, and a 5-h rotation period, we found that a small member of the Themis family with a characteristic radius of 1 km reaches the rotation period of 100 h in ≈ 35 Myr (in the same time the initial obliquity is tilted to its asymptotic value). This is a median time computed over a large number of simulations where we considered 319 objects of YORP type I and type II from our sample of Gaussian random spheres. For each body we performed 500 simulations of the long-term time evolution of the rotation state. We assumed a bulk density of 1.3 g/cm³ and recalibrated the mean distance to the Sun to 3.13 AU. Obviously, the rotation of larger bodies would evolve more slowly, approximately with the square of the characteristic size. A similar result was found also for small members of the Flora family; here the closer proximity to the Sun is compensated by the assumed higher bulk density of the asteroids (≈ 2.5 g/cm³). Such results indicate that the reinitialization of the rotation state of small family members across the whole asteroid belt might be very frequent since the family formed (\approx Gyr or longer in some cases). The influence of the YORP cycles thus needs to be taken into account, or at least estimated, in modeling the long-term dynamical fate of the asteroid families and leakage of kilometer-sized asteroids from the main belt.

3.2. The Role of the Solar Torque and Precession of the Orbit

Apart from the YORP effect and collisions, the gravitational torque due to the Sun represents an additional phenomenon that affects the asteroid spin axis orientation over the long term. (Planetary torques may be relevant for the Earth-crossing population of asteroids, but they are negligible for the main belt asteroids.) Were the orbit fixed in space, the resulting effect of the solar torque would not be important for Yarkovsky applications. Namely, it would consist of a regular precession with frequency ($\approx \alpha \cos \epsilon$, where α is the precession constant “at zero obliquity”) around the normal to the orbital plane, there by leaving the obliquity ϵ constant. Assuming the principal-axis

TABLE I
Estimated Values of the Precession Constant α at Zero Obliquity for Asteroids at Different Location in the Main Belt Compared to the Proper Frequency s of the Nodal Precession Rate

Family	α (″/year)	s (″/year)
Flora	27	35
Eunomia	16	52
Themis	10	103

rotation we have

$$\alpha = \frac{3}{2} \frac{C - (A + B)/2}{C} \frac{n^2}{\omega} \frac{1}{(1 - e^2)^{3/2}}, \quad (8)$$

where (A, B, C) are principal moments of inertia, n is the mean orbital motion, and ω is the proper rotation frequency. The estimated minimum periods of such forced precession range between ≈ 0.3 Myr and several million years, depending on the object’s oblateness, distance from the Sun, and rotation period. Notably, by taking the average value of the dynamical ellipticity $[C - (A + B)/2]/C \approx 0.3$ for small asteroids (Fig. 2) and a 5-h average rotation period we obtain the maximum precession rates α in different parts of the asteroid belt as indicated in the Table I.

The situation is, however, complicated by the fact that the orbital plane is not fixed in space, but it is instead perturbed by the gravitational influence of the planets. The fundamental point here is that some of the frequencies by which the orbit precesses (or oscillates) may be close to the estimated frequency ($\approx \alpha \cos \epsilon$) at which the asteroid spin axis precesses around the orbit due to the solar torque (see Table I). This proximity may cause complex resonant effects and significantly influence the long-term evolution of the spin axis orientation (and thus its obliquity). Even in the cases when the initial forced precession is outside of resonance with the planetary perturbations of the orbit, the underlying slow obliquity and rotation frequency evolution due to the YORP effect may drive the rotation state toward some of the resonances. Bottke *et al.* (2000) noticed the potential importance of the spin axis precession due to the solar torque, though they did not mention explicitly the possibility of the resonance phenomena [see also a previous work by Vokrouhlický and Farinella (1998)]. Here we want to develop the problem in more detail and show the potential complexity of individual rotation histories of asteroids in different parts of the main belt. Our particular aim is to see whether the YORP evolution itself may represent in average the typical rotation history of a small asteroid in the main belt (including the quantitative aspects such as the time scale to drive the rotation to a slow rotation limit).

We should not neglect to mention that the resonant spin axis dynamics has been extensively studied within the context of the long-term evolution of planetary rotation. Following these works, Skoglöv *et al.* (1996) and Skoglöv (1997, 1999) then

applied the same approach to investigation of the rotation state of asteroids. To our mind, the powerful global approach of Laskar and his collaborators (e.g., Laskar and Robutel 1993, Laskar *et al.* 1993, Néron de Surgy and Laskar 1997) is also the most suitable for our application. We thus refer the reader for more details to Laskar and Robutel (1993) and Néron de Surgy and Laskar (1997), while here we just summarize the principal steps and assumptions.

The power of Laskar's approach is mainly that the irrelevant degrees of freedom are eliminated by averaging, while the fundamental degrees of freedom are retained. In the absence of spin-orbital resonances, appropriate for our application, we can thus average over fast proper rotation and revolution around the Sun (as was done for the YORP effect). Considering the effect of the solar gravitational torque only, the fundamental degree of freedom is described by canonically conjugated variables $X = L \cos \epsilon$ and ψ ; here L is the conserved angular momentum of rotation, ϵ is the obliquity, and ψ is the precession in longitude. Note that here we implicitly assume rotation about the principal axis of the inertia tensor, which seems justified for at least multikilometer-sized asteroids (see Section 3.3). It turns out to be suitable to introduce a complex variable $\chi = \sin \epsilon \exp(i\psi)$ (with $i = \sqrt{-1}$), so that $\cos \epsilon = \sqrt{1 - \chi\chi^*}$ (where the star denotes a complex-conjugated quantity). The resulting equations describing the long-term evolution of the spin axis orientation then read (e.g., Laskar and Robutel 1993, Néron de Surgy and Laskar 1997)

$$\frac{d\chi}{dt} = i\chi(\alpha \cos \epsilon - 2\Phi) + \Psi^* \cos \epsilon, \quad (9)$$

with the auxiliary functions

$$\Phi = \frac{1}{2i} \left(\zeta \frac{d\zeta^*}{dt} - \zeta^* \frac{d\zeta}{dt} \right), \quad (10)$$

$$\Psi = \frac{2}{\sqrt{1 - \zeta\zeta^*}} \left(\frac{d\zeta}{dt} - i\zeta\Phi \right). \quad (11)$$

The complex variable $\zeta = \sin(I/2) \exp(i\Omega)$ describes orientation of the orbital plane in space; I is the inclination and Ω is the longitude of the ascending node. If ζ were constant, we easily verify that the solution of (9) is the regular precession of ψ with frequency $\alpha \cos \epsilon$ (and $\epsilon = \text{constant}$). However, the complexity of the problem stems from the fact that ζ is time dependent, describing orbital motion due to planetary perturbations. It may be given by a Fourier series approximation from the analytic theory, or—as in our case—as a purely numerical output from integration of the orbital motion of an asteroid. As a part of another research project we have integrated orbits of hundreds of asteroids in main belt families over hundreds of Millions of years (e.g., Nesvorný *et al.* 2002), and we “borrow” these results for our study of the long-term evolution of their spin axes.

We mention that in our simulations we actually used a slightly modified variable $\chi' = (1 - \cos \epsilon) \exp(i\psi)$ that suitably rele-

gates the coordinate singularity to $\epsilon = 180^\circ$. The corresponding dynamical equations then look a little less compact but they are easily obtained from (9).

Equation (9) can be generalized to include the YORP effect by extending the right-hand side by a term

$$\left(\frac{d\chi}{dt} \right)_{\text{YORP}} = \chi \frac{\bar{T}_\epsilon}{C\omega} \tan \epsilon. \quad (12)$$

The equation $d\omega/dt = \bar{T}_s/C$ [see (3)] should be considered along with this generalized form of (9). Note that the precession constant α from (8) depends on the rotation rate ω , which presents an additional coupling of the resulting system of three differential equations for variables (χ, ω) . Equation (8) apparently suggests $\alpha \propto 1/\omega$; hence increasing the precession constant as the YORP effect asymptotically decelerates the rotation rate, but the exact dependence $\alpha(\omega)$ may be more complicated because the dynamical ellipticity $[C - (A + B)/2]/C$ may also depend on ω . As an example we mention that for planets, with fluid or viscoelastic layers, the rotational deformation leads approximately to $[C - (A + B)/2]/C \propto \omega^2$. For smaller asteroids that are likely to be rubble piles we do not have an exact estimate of the rotational deformation, so that at the zero approximation we shall assume $[C - (A + B)/2]/C \approx \text{constant}$. This should not hold for rotation periods approaching the zero-strength disruption limit by the centrifugal force, which appears to be about 2 h (consistent with the upper limit of the observed rotation periods for asteroids larger than ≈ 200 m in size; Pravec and Harris 2001).

Following the motivation from the end of Section 3.1.5, we next illustrate the complexity of the long-term evolution due to the aforementioned effects for small members of Themis and Flora families. Interested readers may find additional results for small asteroids in the Eunomia family on our Web site <http://sirrah.troja.mff.cuni.cz/~davok/>.

3.2.1. Example: Themis Asteroids

We intentionally start our discussion with Themis, since the effects of the mutual interaction between the gravitational solar torque and the orbital excitations is weak and restricted to isolated events. There are several reasons for this conclusion, the most important of which are (i) small orbital inclination of the Themis asteroids and (ii) a good separation of the proper and forced frequencies by which the orbital plane is perturbed from the estimated precession rate of the spin axis (see Table I). Fourier analysis of the orbital data, namely, the $\zeta = \sin I/2 \exp(i\Omega)$ variable and the Ψ quantity from (11), indicates that in the relevant range of frequencies their spectrum is composed of well-isolated lines (dominant frequencies are the proper frequency $s \approx 103''/\text{year}$ and the forced frequencies $s_6 \approx 25.7''/\text{year}$, $s_7 \approx 2.9''/\text{year}$, and $s_8 \approx 0.7''/\text{year}$ and the relevant sidebands). This suggests a near regularity of the spin axis evolution, except from singular resonant cases. The YORP effect may obviously drive the rotation evolution toward these

resonances, but none of them is expected to trigger a large-scale chaotic motion of the spin axis.

As far as the YORP effect is concerned, we shall use a typical (“average”) result from the Gaussian-sphere sample of kilometer-sized objects discussed in Section 3.1.5 and scale them to the appropriate distance from the Sun. In the Themis case, we also renormalize the assumed mean density of the asteroid to 1.3 g/cm^3 , which better fits the C-type asteroids. The orbital data are taken from a 150-Myr direct numerical integration of a test particle at 3.13 AU (the eccentricity and inclination fits the mean of the Themis family). Gravitational perturbations of the outer planets were included. Our intention is not to investigate all possible results spanning the whole initial data parameter space, such as the initial period, obliquity, precession constant, and so on, but rather to show several examples. A more systematic search is beyond the scope of this paper.

Figure 15 shows one of the possible histories of the rotation state of a 2-km-sized Themis asteroid (with initial data given in the caption of the figure). As in all the examples that follow, we always compare two simulations: (i) a restricted one with only the YORP effect included, and (ii) a more complete simulation including both the YORP effect and the gravitational solar torque. Notice that both models yield very similar results. In the complete model, the obliquity gets only very slightly perturbed as a consequence of the passage through the s_7 resonance (when $d\psi/dt - s_7 \simeq 0$); apart from this small effect the restricted model, containing the YORP effect only, follows the results of the complete model closely. In both cases, we notice the outstanding characteristics of the YORP evolution (see Rubincam 2000). Notably, the obliquity is secularly driven to an asymptotic value of 90° (type I case); given the small initial obliquity, the rotation period is first decreased to about 4 h, while at later epochs of the YORP evolution it rapidly increases. We terminate the simulation when the rotation period reaches 100 h, since our model is inappropriate and incomplete for longer periods for two reasons. First, nondisruptive collisions may easily modify the rotation state at this slow-rotation phase, and second, the averaging method used for modeling the YORP effect may not be applicable when the rotation period becomes a fair fraction of the revolution period. It may also be noticed that about 90 Myr is enough time to reach the near-asymptotic state and tilt the axis by 70° in obliquity. Regarding the size-scaling of the YORP torques, we may conjecture that this time will scale with the square of the characteristic length of the object. For a 10-km-sized asteroid the evolution from Fig. 15 may thus take $\approx 2.25 \text{ Gyr}$.

Figure 16 shows another possible history of the Themis kilometer-sized asteroid rotation. The main difference from the previous example concerns the YORP type; here, the asteroid is assumed to belong to the type II class. The obliquity is then driven to the 0° state. Nevertheless, this expected evolution is temporarily inverted in the complete model due to a capture in s_6 and s resonances; the s_7 resonance is too weak for a capture. Figure 16c clearly illustrates that the precession rate $d\psi/dt$ is

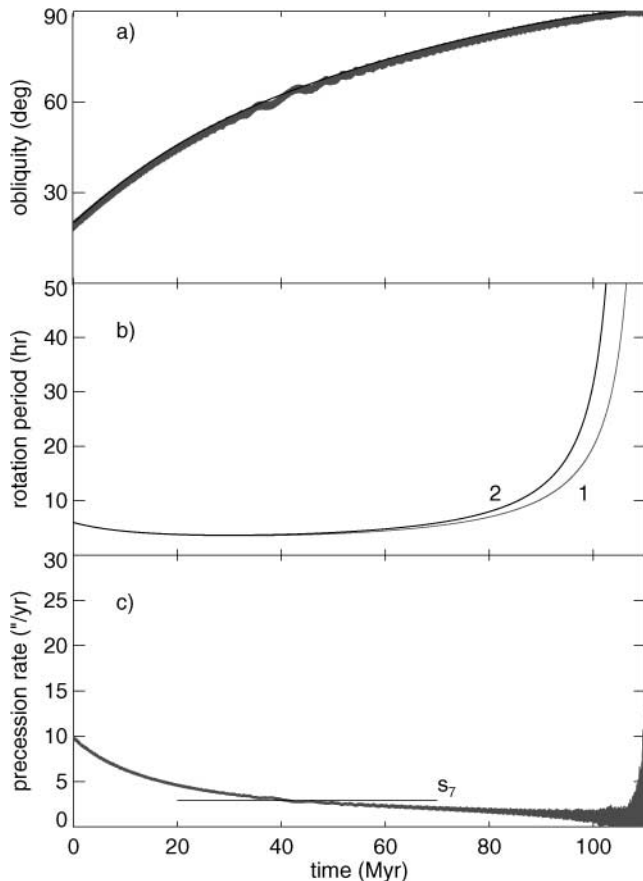


FIG. 15. Long-term evolution of (a) the obliquity ϵ , (b) the rotation period P , and (c) the forced precession frequency $d\psi/dt$ for a typical, kilometer-sized Themis asteroid. The simulation includes the gravitational torque due to the Sun and the YORP effect; initial data are $\epsilon(0) = 20^\circ$, $P(0) = 6 \text{ h}$, and the precession constant $\alpha = 10''/\text{year}$. The black curve (labeled 2) shows evolution with only the YORP effect included, the gray curve (labeled 1) corresponds to evolution with both the YORP effect and the solar gravitational torque. The asteroid orbit evolves due to planetary perturbations. The YORP solution corresponds to type I according to our classification (i.e., driving the spin axis to the orbital plane).

trapped to the resonance value. Since the rotation rate is permanently decayed, the obliquity is forced to decrease, as can be seen between 47 and 56 Myr (Fig. 16a). The situation is similar to a temporary capture of dust particles in the exterior orbital resonances with planets, where eccentricity is forced to increase when the orbit is trapped in the resonance as a result of continuous draining of the angular momentum with “stopped evolution” of the semimajor axis. However, even disregarding such fine details of the evolution, it can still be rather well approximated by the restricted model with the YORP effect. This is true, in particular, with regard to the time scale needed to reach the near-asymptotic state of a very slow rotation.

We have seen in Section 3.1 that the YORP obliquity evolution may asymptotically reach any value in the admissible range. This is the type III case, which is illustrated in Fig. 17. The evolution is fairly similar to that from Fig. 16, with the

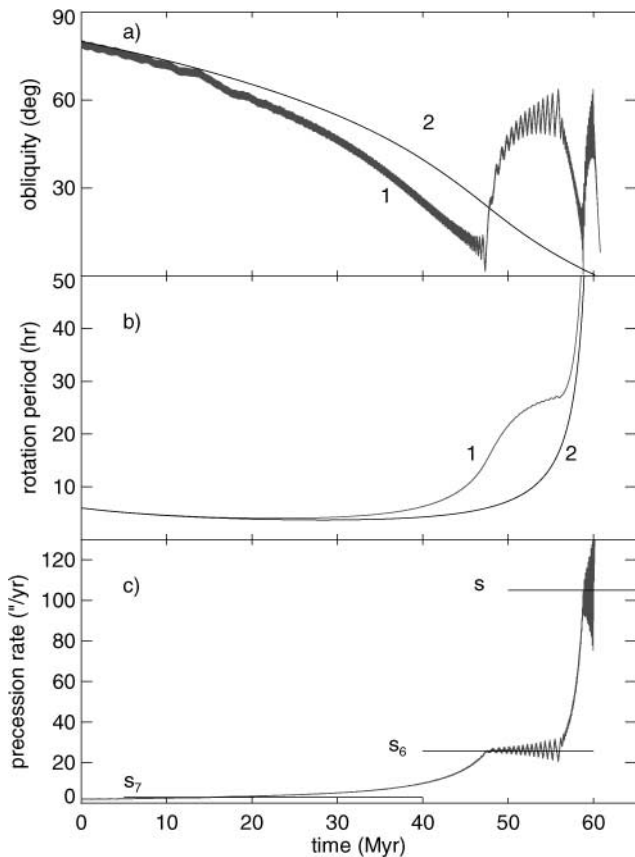


FIG. 16. The same as in the Fig. 15, except for for the initial obliquity $\epsilon(0) = 80^\circ$ and the YORP effect of type II (i.e., the spin axis tends to align with the normal to the orbital plane). Notice that the precession rate $d\psi/dt$ (c) is temporarily captured in the s_6 and s resonances; since the rotation period is constantly increased, the obliquity is forced to resonantly increase (a).

only difference being in the asymptotic value of the obliquity. The s_6 and s resonances temporarily capture the slow increase of the precession rate, but the permanent decrease of the rotation energy eventually releases the evolution from these resonances. The unavoidable slow-rotation late phase will then be interrupted by a collision with a sufficiently large projectile. Resonance captures may not necessarily result in prolonging the spin axis evolution; this is actually seen in Fig. 17, since the complete model evolution to the 100-h rotation period takes some 8 Myr less than in the YORP case only. Compared to the entire ≈ 110 -Myr evolution, this is only a minor effect. However, there are also cases where the resonances may halt the rotation evolution for a more considerable period. Figure 18 shows an example with the underlying YORP effect of type IV. We may notice long-lasting captures in the s_6 and s resonances. As a result, the rotation evolutions to the long-period state takes longer (140 Myr compared to 90 Myr) when only the YORP effect is taken into account.

Despite of the limited number of cases discussed here, we may preliminarily conclude that the YORP evolution itself is

a very good approximation of the complete model. The rare and separated resonances between the forced precession of the spin axis due to the solar torque and the orbital excitations may temporarily affect the smooth YORP evolution, but they do not generally result in a large-scale wandering of the spin axis.

3.2.2. Example: Flora Asteroids

We have repeated the previous examples for the small (kilometer-sized) members of the Flora family. In practice this means that we rescaled the magnitude of the YORP-averaged torques to the 2.2 AU distance from the Sun and we used a numerically integrated orbit of the asteroid Flora over a 140-Myr timespan. We assumed a mean density of 2.5 g/cm^3 , conformal to the S-type asteroids. The closer proximity to the Sun results in two important differences if compared to the Themis case: (i) since the orbit is further from Jupiter, the proper nodal frequency s is smaller (see Table I) and gets close to the forced frequencies (especially $s_6 \approx 25.7''/\text{year}$), and (ii) since the revolution period is shorter, the precession constant α increases for a typical Flora asteroid to approximately the s_6 value. The first item means that the Fourier spectrum of the ζ and Ψ variables

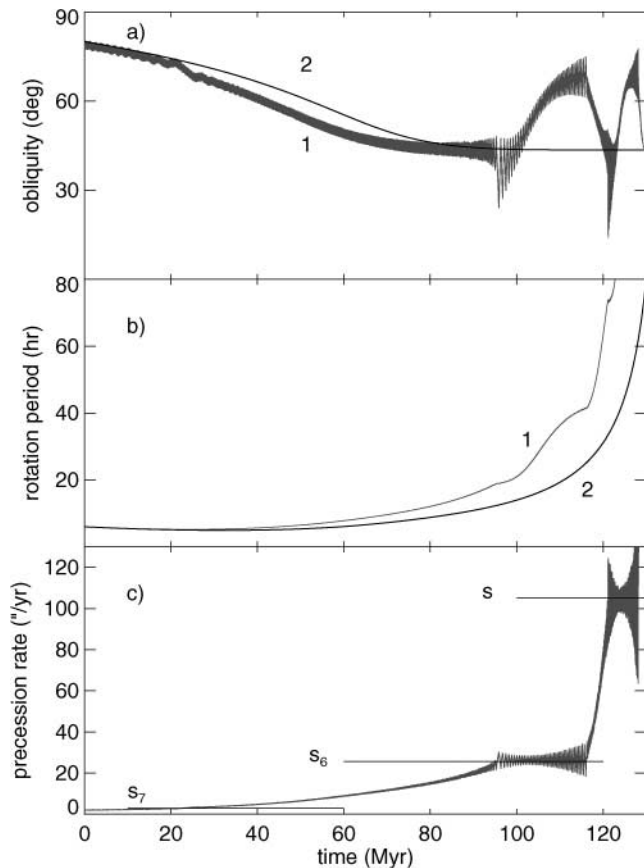


FIG. 17. The same as in the Fig. 15, except for the initial obliquity $\epsilon(0) = 80^\circ$ and the YORP effect of type III (i.e., the obliquity is asymptotically driven to an intermediate value of $\approx 44^\circ$).

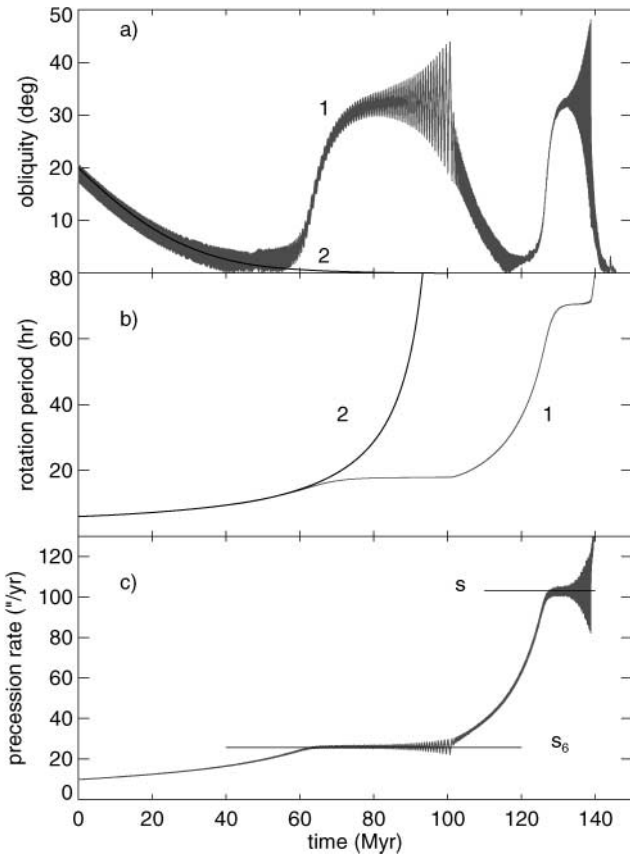


FIG. 18. The same as in the Fig. 15, except for the YORP effect of type IV (i.e., the spin axis asymptotically driven either to the orbital plane or into alignment with its normal depending on the initial value of the obliquity; in this case it approaches the 0-obliquity state).

is no longer composed of well-isolated lines, but the bulk of the signal is poorly periodic and the spectrum contains clusters of lines [compare, e.g., with the spectrum of *A* and *B* variables for Mars from Laskar and Robutel (1993)]. The resonances may “communicate” with each other and drive the precession rate $d\psi/dt$ over a larger range. Such a chaotic wandering of ψ may trigger a similar effect in the obliquity, as has been found by Laskar and his collaborators for most of the inner planets and Skoglöv for some asteroids. The second item mentioned here means that the typical precession rates for the Flora asteroids should be located close to these resonance clusters. As a result of this qualitative insight, we may expect a less regular evolution of the obliquity than in the Themis case. Additionally, higher inclination of the Flora orbits may cause larger oscillations of the obliquity.

Figure 19 formally corresponds to the same initial data as in Fig. 15, except with the Flora orbit and YORP parameters. Apart from larger amplitude oscillations of the obliquity (and the precession rate), the results are comparable. The YORP evolution itself corresponds rather well to the complete model result. Interestingly, the time scale needed to reach the asymptotic,

slow-rotation state is approximately the same as in the Themis case (see also results in Sections 3.1.5); the larger radiation flux in the Flora zone is roughly compensated for by a higher mean density of the Flora S-type asteroids.

Figure 20 shows a more perturbed case of the possible Flora-asteroid rotation history, notably corresponding formally to the same initial data as in Fig. 16. A type II YORP effect drives the alignment with the orbital angular momentum at late epochs of the evolution, which—together with the secularly decelerated rotation rate—means that the precession rate encounters the large resonance zone. When this occurs (at ≈ 22 Myr), the obliquity undergoes large oscillations. Figure 16c indicates that the evolution alternates in a random way between the nearby s_6 and s resonances. Eventually, the resonance lock is interrupted and the evolution quickly heads the slow-rotation phase. The entire timespan is shortened about 25% compared with the YORP-only evolution.

Significant obliquity perturbations may be also seen in Fig. 21, the Flora counterpart of the Themis simulation shown in Fig. 17. Here, the obliquity approaches an intermediate asymptotic value of about 44° and the resonance phenomena in the complete model largely mask the smooth YORP-only evolution. In

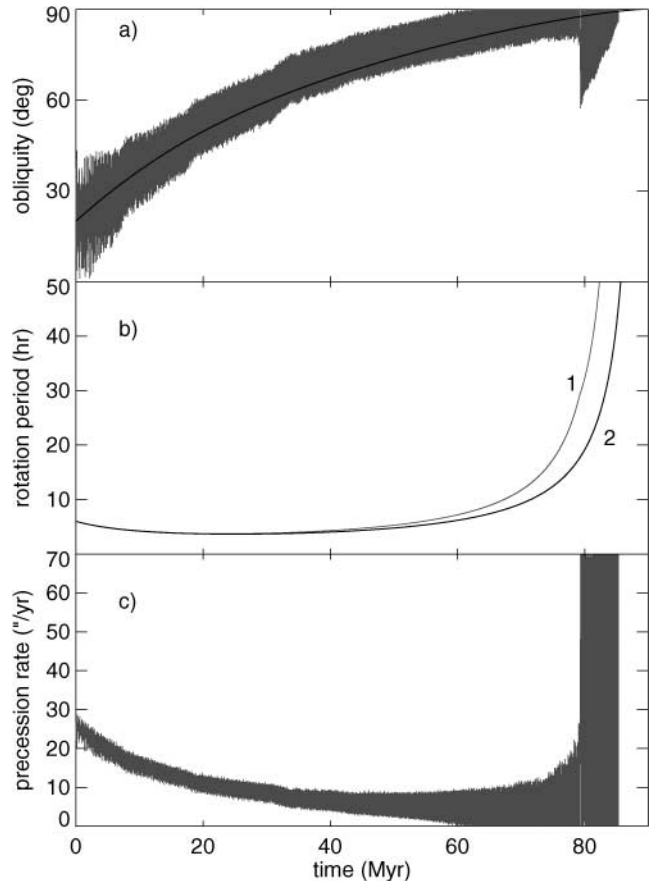


FIG. 19. The same as in the Fig. 15, except for a kilometer-sized Flora asteroid.

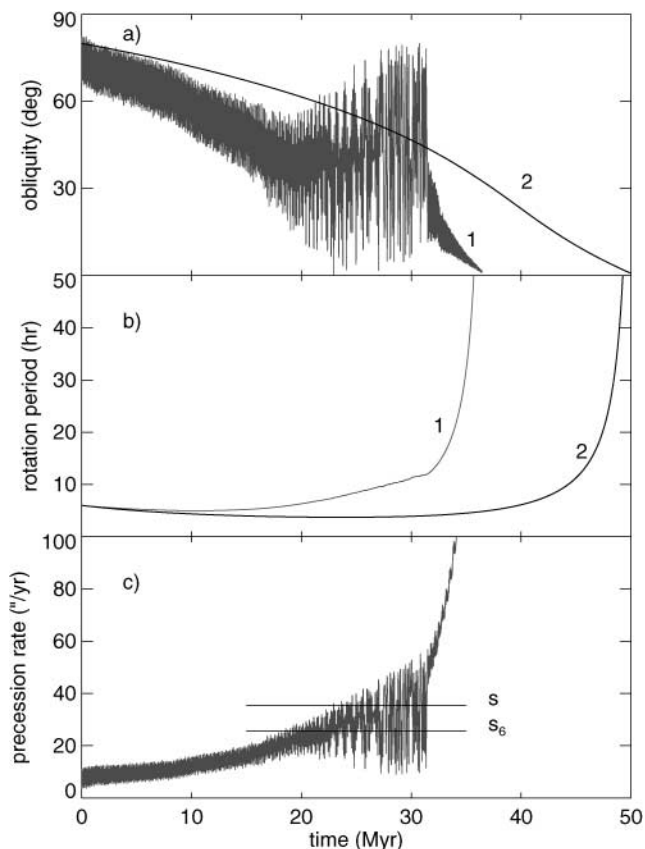


FIG. 20. The same as in the Fig. 16, except for a kilometer-sized Flora asteroid.

contrast to the previous example, the resonance effects delay the rotation evolution toward the long-period phase by some 20%. It is, however, very important to notice that despite the difference in the obliquity evolution, the accumulated Yarkovsky change in the semimajor axis would differ by only $\approx 10\%$. This actually applies also to the example shown in Fig. 20, since the shorter evolution is partially compensated for by a smaller obliquity (in average), which increases the semimajor axis drift for the diurnal variant of the Yarkovsky effect.

Our final example, Fig. 22, demonstrates a less frequent case when the rotation histories as given by the complete and YORP-only models are significantly different. This is the case of the type IV YORP effect, which may be asymptotically driven either to 0° or 90° obliquity depending on its initial value. The chosen initial data (namely, 20° for the obliquity) are nominally attracted by the 0° -obliquity asymptotic state if only the YORP effect is assumed. However, the large oscillations of the obliquity caused by the s_6 resonance may invert this evolution and drag the obliquity toward the complementary asymptotic value of 90° . This case is actually seen in the evolution presented in the Fig. 22 (we stopped the simulation at 140 Myr since this is the time interval over which we have the orbital data). We should, however, comment that this last example is statistically

less frequent (see Section 3.1.5 where we found that the type IV YORP objects comprise only $\approx 6\%$ of all bodies).

3.3. Comments on Inelastic Relaxation of the Tumbling State of Rotation

The assumption of rotation around the principal axis of the inertia tensor is one of many approximations we adopted in this paper. A single periodicity of lightcurves of most asteroids does suggest that this is a commonly satisfied situation, but in some cases we have evidence for non-principal-axis (tumbling) rotation (e.g., Toutatis and Comet Halley). We have seen the YORP effect implies at least two reasons for analyzing whether the principal-axis rotation is appropriate for small asteroids: (i) the YORP effect naturally produces torque components, which drive the rotation out of the fundamental-energy state, and (ii) even if (i) is weak the predicted long-term evolution of the asteroidal rotation due to the YORP effect may include a final slow-rotation phase, interrupted eventually by a larger collisional event that may increase the rotation rate. After undergoing such an event, the asteroid rotation should be generically placed in an excited (tumbling) state. On the other hand, inelastic processes tend to dissipate the energy of the wobble. A comparison of a characteristic time scale for such dissipative processes with that

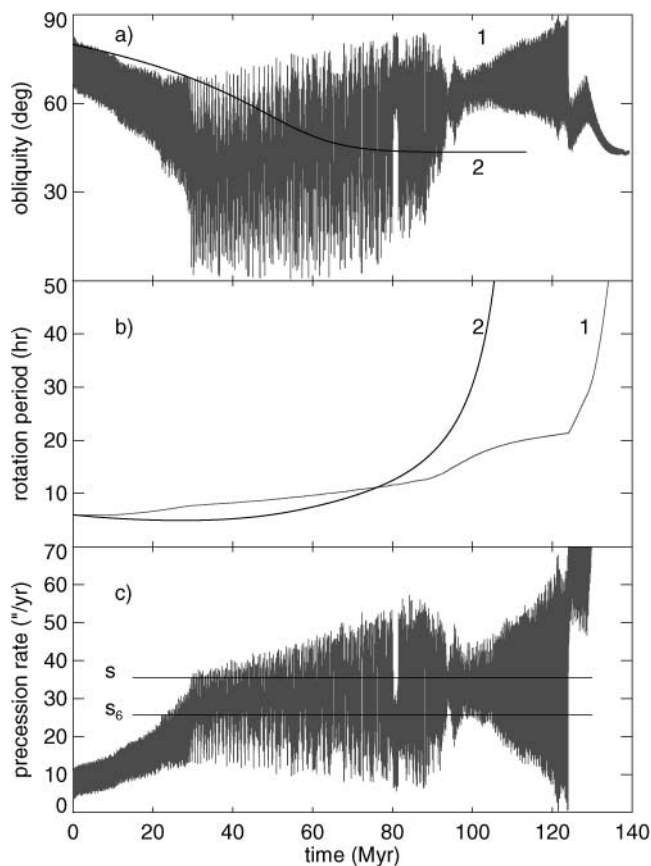


FIG. 21. The same as in the Fig. 17, except for a kilometer-sized Flora asteroid.

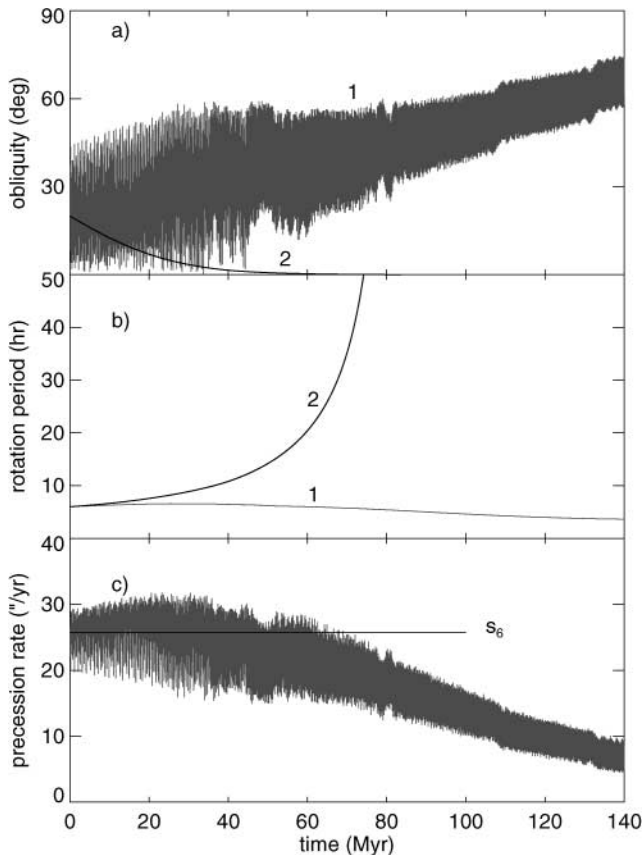


FIG. 22. The same as in the Fig. 18, except for a kilometer-sized Flora asteroid.

of the YORP evolution is then of fundamental importance for understanding whether the principal-axis rotation assumption is justified (over at least a major part of the YORP evolution). Rubincam (2000) noted these facts and here we are try to elaborate the corresponding estimations in somewhat more detail.

Free precession of a rotating body causes alternating stresses in its interior. A variety of processes, such as unpinning of dislocations, sliding at grain boundaries, or interaction of internal faults, then result in irreversible dissipation of the rotation energy, which is thus damped toward the minimum state of rotation around the principal axis of inertia tensor. Since a detailed modeling of such molecular-level microscopic processes is very complicated, if not impossible, one usually characterizes the energy dissipated over one alternating cycle of internal forces by an empirical quality factor Q . Its value has been determined from a number of astronomical observations and laboratory measurements for a variety of materials and frequencies of their excitations. It has been indeed found that the Q values are compositional and frequency dependent. Relevant periods at which asteroidal interiors are strained range from about half a day to several days (excluding the slowly rotating population of asteroids). Not only do we lack any direct observational calibration of the quality factor for asteroids, but also the values obtained

by different techniques typically occur at different frequencies and for different composition than the presumed rubble piles for small asteroids. The quality factor Q is thus largely uncertain in our application; admissible values range from about 100 (or even less) to about 300. The upper value is consistent with the high-frequency determinations for lithospheric rocks (both in the laboratory and from the free modes of Earth oscillations). At lower frequencies, Q typically decreases, satisfying roughly a power law, down to about 30 for Earth tides (monthly and semimonthly periods). A value of $Q \approx 100$ –150 thus seems to be likely for small, rubble-pile asteroids with strain periods of a few days; this value is also commonly adopted for the small planetary satellites (e.g., Peale 1999). The low-rigidity C types may have even a slightly smaller Q , conformal to the assumed value for Comet Halley.

Burns and Safronov (1973) determined, from general principles and qualitative reasoning, that the characteristic time scale to dissipate the free-precession energy is

$$T \approx \kappa \frac{\mu Q}{\rho R^2 \omega^3}, \quad (13)$$

where R is the radius, ω is the rotation frequency, and μ is the rigidity (or shear elastic modulus) of the asteroid. The major uncertainty here follows from inaccurate knowledge of (i) the quality factor Q (as already mentioned), (ii) the numerical coefficient κ , and to some extent (iii) the rigidity μ . This numerical coefficient κ depends on the geometry of the body and the frequency spectrum of the internal strain. There has recently been some discussion about the appropriate value of κ (e.g., Lazarian and Efroimsky 1999, Efroimsky and Lazarian 2000, Efroimsky 2000), with a tendency for smaller values being favored. Burns and Safronov (1973) determined $\kappa \approx 10$ –100 (cgs units), depending on the sphericity of the asteroid (upper value for near spherical objects), while Efroimsky and Lazarian (2000) advocate a value $\kappa \approx 4$ –5. Though the latter authors seem to rightly point out the importance of the second harmonic of the wobble frequency, the difference in κ is ultimately not that fundamental given the degree of other simplifications. Moreover (J. A. Burns, private communication), the very low κ results still need to be confirmed by a direct numerical model of a strained, rotating, inelastic body (with currently controversial conclusions). We shall thus assume $\kappa \approx 20$ in the following estimations. As for the rigidity, we shall assume $\approx 5 \times 10^{11}$ dyne/cm² for the silicate asteroids (S types), which is consistent with laboratory measurements of elastic moduli of the ordinary chondrites (e.g., Yomogida and Matsui 1983). Actually, this value fits the data of H-chondrites, while L-chondrites have μ typically somewhat smaller. For asteroids located in the outer belt (C types) we assume a smaller value $\approx 5 \times 10^{10}$ dyne/cm², fitting approximately the cometary data (with $Q \approx 100$ this is about what other authors suggest; e.g., Jewitt 1997). We thus obtain the following characteristic time scales for relaxation of the free wobble due to the inelastic internal processes: $T \approx 0.36 \times (P_{\text{hr}}^3/R_{\text{km}}^2)$ for S types

and $T \approx 0.04 \times (P_{\text{hr}}^3/R_{\text{km}}^2)$ for C types (here P_{hr} is the rotation period in hours, R_{km} is the radius in kilometers, and T is then given in millions of years). Harris (1994) also considered the problem of the tumbling asteroids and obtains $T \approx 0.05 \times (P_{\text{hr}}^3/R_{\text{km}}^2)$ in average. This is slightly less than our value for S types, because this author assumed a smaller value of μQ . Taking our estimates and 5 h for the typical rotation period of kilometer-sized asteroids (excluding slow rotators like Mathilde or Toutatis; see, e.g., Pravec and Harris 2001), we have a damping time scale of ≈ 45 Myr for the S-type and ≈ 5 Myr for the C-type asteroid of $R_{\text{km}} \approx 1$. Since the average rotation rate is approximately constant in the 1–10 range of R_{km} , the estimated damping time scales diminish as $\propto 1/R_{\text{km}}^2$ in this range of interest.

A comparison with the estimated YORP time scales (e.g., from the statistical result in Section 3.1.5 or the examples in Section 3.2) indicates that the C-type kilometer-sized asteroids might relax toward the fundamental state of rotation around the principal axis of rotation on a time scale shorter than that of YORP evolution. So, as an example, assuming a YORP model with principal axis rotation might be rather well justified for Themis kilometer-sized members. On the other hand, the smallest Flora members may have a damping time scale comparable to (or even longer than) their YORP evolution time scale and we should consider modeling of YORP with some precaution. However, if we would consider Harris's (1994) estimate for the tumbling relaxation, the principal-axis rotation would be well justified even for the small Flora asteroids. We thus tentatively conclude that the simplifying assumption of the principal-axis rotation is rather well justified, being obviously violated only for the unusual, slow-rotation population of asteroids.

4. CONCLUSIONS

The main results of this paper can be summarized as follows:

- We have investigated the role of the thermal radiation torque on the long-term rotation history of small asteroids (up to ≈ 10 km in size). Except for the unrealistic cases of spherical bodies and perfect ellipsoids, this torque always secularly affects the rotation; in particular the obliquity is slowly driven to some asymptotic value while the rotation period typically secularly increases (a permanent decrease of the rotation period is also possible, but this is statistically less frequent). Four principal approximations were assumed in this text: (i) applicability of the averaging principle, (ii) zero thermal relaxation of the asteroidal surface, (iii) circular orbits (this assumption, however, just conveniently constrains the parameter space of the solutions and does not present a theoretical limitation of our approach), and (iv) the principal-axis rotation state.
- By analysing the functional dependence of the obliquity-affecting torque \bar{T}_e on the obliquity value, we have classified possible cases of the YORP-induced evolution of the obliquity.

- The YORP torques were computed for 10 shapes of real objects (nine asteroids and Deimos) and also for a large sample of synthetic objects generated by the Gaussian random sphere technique. Since the Gaussian model parameters were fitted to the known shapes of small asteroids, the sample is assumed to well represent the shape characteristics of small Solar System bodies. As a result we were able to estimate a statistically averaged YORP influence on small members of Themis and Flora asteroid families for such properties as the characteristic time scale to reach the asymptotic, slow-rotation regime. This finding is important for improving models of slow semimajor axis dispersion in asteroid families.

- As a particular result, we predict that the YORP effect may be directly observable through change of the rotation frequency of the small near-Earth asteroid 1998KY26 during its next close approach in May 2024.

- If YORP were the only cause of the long-term evolution of the asteroid rotation state, it would drive the obliquity to some particular value (depending on the type). When this value of the obliquity is reached, and the averaging approach is still applicable, the rotation frequency is preferentially decreased. This is a result from the sample of 500 Gaussian random spheres. The less likely case of a permanent spinning up of the body may occur, and we found it, as an example, for an object of Castalia's shape.

- In addition to the slow YORP-induced evolution of the rotation state, we include in our model the influence of the gravitational torque due to the Sun. Since the orbital elements evolve in time due to planetary perturbations, the forced precession of the spin axis may resonantly beat with the orbital excitations. This is indeed the case of small asteroids, with sizes larger than several hundred meters across and with slow enough rotation (\approx hours). We illustrate the obliquity effects triggered by such resonant phenomena. The YORP effect may drive the nonresonant states toward the resonances. Meteoroid precursors, with sizes up to tens of meters, presumably rotate fast enough so that the precession rate due to the solar torque is significantly different (smaller) than the orbital excitation. The resonant effects studied in this text are thus likely to be unimportant for these very small objects in the Solar System.

- The assumption of principal-axis rotation seems well justified in average for multikilometer-sized asteroids; however, the kilometer-sized objects may relax toward the principal-axis rotation state slowly. The YORP torque may also continuously drive the rotation state away from the fundamental state of rotation. These effects need to be studied in the future.

A major issue omitted in this paper concerns the role of collisions within the model we investigated. Yet, collisions are necessarily an inherent part of the model, since they must tune the limit to which the asteroids decelerate their rotation rate by the YORP effect. Inclusion of the collisional processes, however, represents an entirely new and vast dimension to the studied problem and we feel that this would already go beyond this introductory paper of the series. We certainly need to return to this issue in the future.

ACKNOWLEDGMENTS

We are grateful to J. Ďurech for indicating to us the importance of the Gaussian random sphere approach by Muinonen; D. Nesvorný is thanked for letting us use available data of his 140-Myr orbital integration of the asteroid Flora. J. Spitale, as a referee, helped to improve the final form of this paper.

REFERENCES

- Bottke, W. F., D. C. Richardson, P. Michel, and S. G. Love 1999. 1620 Geographos and 433 Eros: Shaped by planetary tides? *Astron. J.* **117**, 1921–1928.
- Bottke, W. F., D. P. Rubincam, and J. A. Burns 2000. Dynamical evolution of main belt meteoroids: Numerical simulations incorporating planetary perturbations and Yarkovsky thermal forces. *Icarus* **145**, 301–330.
- Bottke, W. F., D. Vokrouhlický, M. Brož, and A. Morbidelli 2001a. *Yarkovsky-Assisted Escape of Kilometer-Sized Asteroids from the Main Belt*. Presented at *Asteroids 2001*, Palermo, Italy.
- Bottke, W. F., D. Vokrouhlický, M. Brož, D. Nesvorný, and A. Morbidelli 2001b. Dynamical spreading of asteroid families via the Yarkovsky effect: The Koronis family and beyond. *Science* **294**, 1693–1696.
- Burns, J. A., and V. S. Safronov 1973. Asteroid nutation angles. *Mon. Not. R. Astron. Soc.* **165**, 403–411.
- Dobrovolskis, A. R. 1996. Inertia of any polyhedron. *Icarus* **124**, 698–704.
- Ďurech, J. 2002. Shape determination of the Asteroid (6053) 1993 BW₃. *Icarus*, in press.
- Efroimsky, M. 2000. Precession of a freely rotating rigid body. Inelastic relaxation in the vicinity of poles. *J. Math. Phys.* **41**, 1854–1888.
- Efroimsky, M., and A. Lazarian 2000. Inelastic dissipation in wobbling asteroids and comets. *Mon. Not. R. Astron. Soc.* **311**, 269–278.
- Farinella, P., and D. Vokrouhlický 1999. Semimajor axis mobility of asteroidal fragments. *Science* **283**, 1507–1511.
- Farinella, P., D. R. Davis, P. Paolicchi, A. Cellino, and V. Zappalà 1992. Asteroid collisional evolution: An integrated model for the evolution of asteroid rotation rates. *Astron. Astrophys.* **253**, 604–614.
- Farinella, P., D. Vokrouhlický, and W. K. Hartmann 1998. Meteorite delivery via Yarkovsky orbital drift. *Icarus* **132**, 378–387.
- Giblin, I., and P. Farinella 1997. Tumbling fragments from experiments simulating asteroidal catastrophic disruption. *Icarus* **127**, 424–430.
- Harris, A. W. 1979. Asteroid rotation rates. II. A theory for the collisional evolution of rotation rates. *Icarus* **40**, 145–153.
- Harris, A. W. 1994. Tumbling asteroids. *Icarus* **107**, 209–211.
- Hartmann, W. K., P. Farinella, D. Vokrouhlický, S. J. Weidenschilling, A. Morbidelli, F. Marzari, D. Davis, and E. Ryan 1999. Reviewing the Yarkovsky effect: New light on the delivery of stone and iron meteorites from the asteroid belt. *Meteorit. Planet. Sci.* **34**, A161–A168.
- Jewitt, D. 1997. Cometary rotation: An overview. *Earth, Moon, Planets* **79**, 35–53.
- Klinkrad, H., Ch. Koeck, and P. Renard 1990. Precise satellite skin-force modelling by means of Monte-Carlo ray tracing. *ESA J.* **14**, 409–430.
- Laskar, J., and P. Robutel 1993. The chaotic obliquity of the planets. *Nature* **361**, 608–612.
- Laskar, J., F. Joutel, and F. Boudin 1993. Orbital, precessional, and insolation quantities for the Earth from –20 Myr to +10 Myr. *Astron. Astrophys.* **270**, 522–533.
- Lazarian, A., and M. Efroimsky 1999. Inelastic dissipation in a freely rotating body: Application to cosmic dust alignment. *Mon. Not. R. Astron. Soc.* **303**, 673–684.
- Love, S. G., and T. J. Ahrens 1997. Origin of asteroid rotation rates in catastrophic impacts. *Nature* **386**, 154–156.
- Muinonen, K. 1996. Light scattering by Gaussian random particles. *Earth, Moon, Planets* **72**, 339–342.
- Muinonen, K. 1998. Introducing the Gaussian shape hypothesis for asteroids and comets. *Astron. Astrophys.* **332**, 1087–1098.
- Muinonen, K., and J. S. V. Lagerros 1998. Inversion of shape statistics for small Solar System bodies. *Astron. Astrophys.* **333**, 753–761.
- Néron de Surgy, O., and J. Laskar 1997. On the long term evolution of the spin of the Earth. *Astron. Astrophys.* **318**, 975–989.
- Nesvorný, D., A. Morbidelli, D. Vokrouhlický, W. F. Bottke, and M. Brož 2002. The Flora family: A case of the dynamically dispersed collisional swarm? *Icarus* **157**, 155–172.
- Ostro, S. J., J. F. Chandler, A. A. Hine, K. D. Rosema, I. I. Shapiro, and D. K. Yeomans 1990. Radar images of asteroid 1989 PB. *Science* **248**, 1523–1528.
- Ostro, S. J., and 15 colleagues 1999a. Asteroid 4179 Toutatis: 1996 radar observations. *Icarus* **137**, 122–139.
- Ostro, S. J., and 19 colleagues 1999b. Radar and optical observations of Asteroid 1998 KY26. *Science* **285**, 557–559.
- Paddack, S. J. 1969. Rotational bursting of small celestial bodies: Effects of radiation pressure. *J. Geophys. Res.* **74**, 4379–4381.
- Peale, S. J. 1999. Origin and evolution of the natural satellites. *Annu. Rev. Astron. Astrophys.* **37**, 533–602.
- Pravec, P., and A. W. Harris 2001. Fast and slow rotation of asteroids. *Icarus* **148**, 12–20.
- Radzievskii, V. V. 1954. A mechanism for the disintegration of asteroids and meteorites. *Dokl. Acad. Nauk SSSR* **97**, 49–52.
- Rubincam, D. P. 1995. Asteroid orbit evolution due to thermal drag. *J. Geophys. Res.* **100**, 1585–1594.
- Rubincam, D. P. 1998. Yarkovsky thermal drag on small asteroids and Mars–Earth delivery. *J. Geophys. Res.* **103**, 1725–1732.
- Rubincam, D. P. 2000. Radiative spin-up and spin-down of small asteroids. *Icarus* **148**, 2–11.
- Rubincam, D. P., B. F. Chao, and P. C. Thomas 1995. The gravitational field of Deimos. *Icarus* **114**, 63–67.
- Simonelli, D. P., P. C. Thomas, B. T. Carcich, and J. Veverka 1993. The generation and use of numerical shape models for irregular Solar System objects. *Icarus* **103**, 49–61.
- Skoglöv, E. 1997. Evolution of the obliquities for nine near-Earth asteroids. *Planet. Space Sci.* **45**, 439–447.
- Skoglöv, E. 1999. Spin vector evolution for inner Solar System asteroids. *Planet. Space Sci.* **47**, 11–22.
- Skoglöv, E., P. Magnusson, and M. Dahlgren 1996. Evolution of the obliquities for 10 asteroids. *Planet. Space Sci.* **44**, 1177–1183.
- Vokrouhlický, D. 1998. Diurnal Yarkovsky effect as a source of mobility of meter-sized asteroidal fragments. I. Linear theory. *Astron. Astrophys.* **335**, 1093–1100.
- Vokrouhlický, D. 1999. A complete linear model for the Yarkovsky thermal force on spherical asteroid fragments. *Astron. Astrophys.* **344**, 362–366.
- Vokrouhlický, D., and W. F. Bottke 2001. The Yarkovsky thermal force on small asteroids and their fragments. Choosing the right albedo. *Astron. Astrophys.* **371**, 350–353.
- Vokrouhlický, D., and P. Farinella 1998. The Yarkovsky seasonal effect on asteroidal fragments: A nonlinearized theory for the plane-parallel case. *Astron. J.* **116**, 2032–2041.
- Vokrouhlický, D., and P. Farinella 2000. Efficient delivery of meteorites to the Earth from a wide range of asteroid parent bodies. *Nature* **407**, 606–608.
- Vokrouhlický, D., A. Milani, and S. R. Chesley 2000. Yarkovsky effect on small near-Earth asteroids: Mathematical formulation and examples. *Icarus* **148**, 117–146.
- Vokrouhlický, D., M. Brož, P. Farinella, and Z. Knežević 2001. Yarkovsky-driven leakage of Koronis family members, I. The case of 2953 Vyshelevia. *Icarus* **150**, 78–93.
- Yeomans, D. K., and 15 colleagues 2000. Radio science result during the NEAR–Shoemaker spacecraft rendezvous with Eros. *Science* **289**, 2085–2088.
- Yomogida, K., and T. Matsui 1983. Physical properties of ordinary chondrites. *J. Geophys. Res.* **88**, 9513–9533.